Gulf

GULF GENERAL ATOMIC

AEC RESEARCH AND
DEVELOPMENT REPORT

GA-11004
C-93b, Advanced Concepts
for Future Application -
Conversion Devices
M-3679 (65th Ed.)

(U) POST-OPERATIONAL EXAMINATIONS OF TWO CARBIDE-FUELED IN-PILE CONVERTERS

by

L. Yang, M. H. Horner and F. L. Cochran

Prepared under
Contract AT(04-3)-167
Project Agreement No. 14
for the
San Francisco Operations Office
U. S. Atomic Energy Commission

This report contains no defense information other than restricted data and is releasable under the Access Permit Program.

September 30, 1970

GULF GENERAL ATOMIC COMPANY, P.O. BOX 608, SAN DIEGO, CALIFORNIA 92112

DISCLAIMER

~~UNCLASSIFIED~~ ~~CONFIDENTIAL~~

Copy No. 33

GULF GENERAL ATOMIC

AEC RESEARCH AND
DEVELOPMENT REPORT

GA-11004
C-93b, Advanced Concepts
for Future Application -
Conversion Devices
M-3679 (65th Ed.)

(U) POST-OPERATIONAL EXAMINATIONS OF TWO CARBIDE-FUELED IN-PILE CONVERTERS

by

L. Yang, M. H. Horner and F. L. Cochran

SPECIAL REREVIEW FINAL DETERMINATION	Reviewers	Class.	Date
Class: U	RBM	U	03/03/82
	KAW	U	03/04/82

Prepared under
Contract AT(04-3)-167
Project Agreement No. 14
for the
San Francisco Operations Office
U. S. Atomic Energy Commission

~~UNCLASSIFIED~~

GROUP-1
Excluded from automatic downgrading and declassification

RESTRICTED DATA
THIS DOCUMENT CONTAINS RESTRICTED DATA AS DEFINED IN THE ATOMIC ENERGY ACT OF 1954. ITS TRANSMITTAL OR THE DISCLOSURE OF ITS CONTENTS IN ANY MANNER TO AN UNAUTHORIZED PERSON IS PROHIBITED.

Classification cancelled ~~or changed to~~ after 6/5/13
by authority of Gulf, Pat Quinlan, SEC. Asst
by GG TIC, date 12/26/13
~~Gulf General Atomic~~
Project 4022 SFO Patent Cleared 12/19/13

DISTRIBUTION OF THIS DOCUMENT IS UNLIMITED

September 30, 1970

GULF GENERAL ATOMIC COMPANY, P.O. BOX 608, SAN DIEGO, CALIFORNIA 92112

~~DISTRIBUTION OF THIS DOCUMENT IS LIMITED~~
To Government Agencies and Their Contractors Only

~~CONFIDENTIAL~~

This page intentionally left blank.

ABSTRACT

Two 90UC-10ZrC fueled converters, IC-I3 of Mark VI configuration and IC-C3 of Mark VIIB configuration, were examined in hot cell after in-pile operation. IC-I3 operated for 4395 hours at an average emitter temperature of 1675°C as a converter test and then for 2948 hours at an average emitter temperature of ~1500°C as a fuel irradiation test; the average fuel burnup achieved was 2.5×10^{20} fission /c.c. IC-C3 operated 5445 hours at an average emitter temperature of 1670°C as a converter test; the average fuel burnup achieved was 5×10^{19} fission/c.c. The carbide fuel contained 4 wt% tungsten and had a C/U atom ratio of 1.05. Other unique features for the converter components were fluoride tungsten claddings of controlled fluorine contents (18 ppm for IC-I3 and 19 ppm for IC-C3), and the presence of a high temperature seal and a graphite sorption cesium reservoir in IC-C3 converter. The results obtained on fuel swelling, emitter deformation, fuel-cladding interaction and microstructures of various converter components are presented. Solutions to the problem areas encountered are recommended.

CONTENTS

LIST OF FIGURES

TABLES

INTRODUCTION

This report describes the hot cell examination results obtained on two 90UC-10ZrC fueled converters, IC-I3 and IC-C3, after in-pile operation. Table 1 summarizes the component materials and operational histories of these two converters. Figures 1 and 2 show schematically the arrangements of the components in these converters. The unique features are

(1) Both converters are fueled with tungsten-containing 90UC-10ZrC of controlled stoichiometry.

(2) Both converters contain fluoride tungsten cladding of controlled fluorine contents.

(3) Converter IC-C3 contains a 40Nb-60V brazed insulator seal and a graphite sorption reservoir.

(4) Converter IC-C3 is the first Mark VIIB converter fueled with carbide.

This represents the first time such new component materials and carbide fueled Mark VIIB emitter have been subject to hot cell examinations. The information generated should be useful for developing converter component materials for nuclear thermionic application.

TABLE 1

COMPONENTS AND OPERATIONAL HISTORIES OF CONVERTERS IC-I3 AND IC-C3

Converter	Fueled Emitter Configuration	Fuel	Cladding	Collector	Seal	Cesium Reservoir	Operation History	Estimated Burnup (fission/c.c.)	Reason For Termination of Converter Test
IC-I3	Mark VI, 1 inch length, 5/8 inch diameter, tungsten fuel pedestal, two tungsten thermocouple wells	90UC-10ZrC*, C/U atom ratio=1.05, tungsten conc. = 4 wt%	Fluoride tungsten, 50 mil thickness, fluorine content = 18 ppm	Molybdenum	Lucalox-Nb, Litton metallizing layer, Cu-10 Ni braze	Liquid	4395 hrs. as converter test at 1675°C average emitter temperature, 2948 hours as fuel irradiation test at average emitter temperature ~1500°C	2.5×10^{20}	Leakage of argon gas from primary containment into inter-electrode space.
IC-C3	Mark VIIB, 2 inch length, 1.1 inch diameter, no fuel pedestal, two tungsten thermocouple wells	90UC-10ZrC**, C/U atom ratio=1.05, tungsten conc. = 4 wt%	Fluoride tungsten, 40 mil thickness, fluorine content = 19 ppm	Niobium	Lucalox-Nb, W-Y_2O_3 metallizing layer, 40Nb-60V braze	Graphite sorption	5445 hrs. as converter test at 1670°C average emitter temperature	5×10^{19}	Leakage of helium gas from primary containment into inter-electrode space

*The fuel body consists of four right cylinders. Each cylinder is 1/4 inch in height and contains 16 holes of 25 mil diameter and a central cylindrical cavity of 0.130 inch diameter to facilitate fission gas venting.

**The fuel body consists of eight cylindrical wafers. Each wafer is 1/8 inch in height and contains a central cylindrical cavity of 0.312 inch diameter to facilitate fission gas venting.

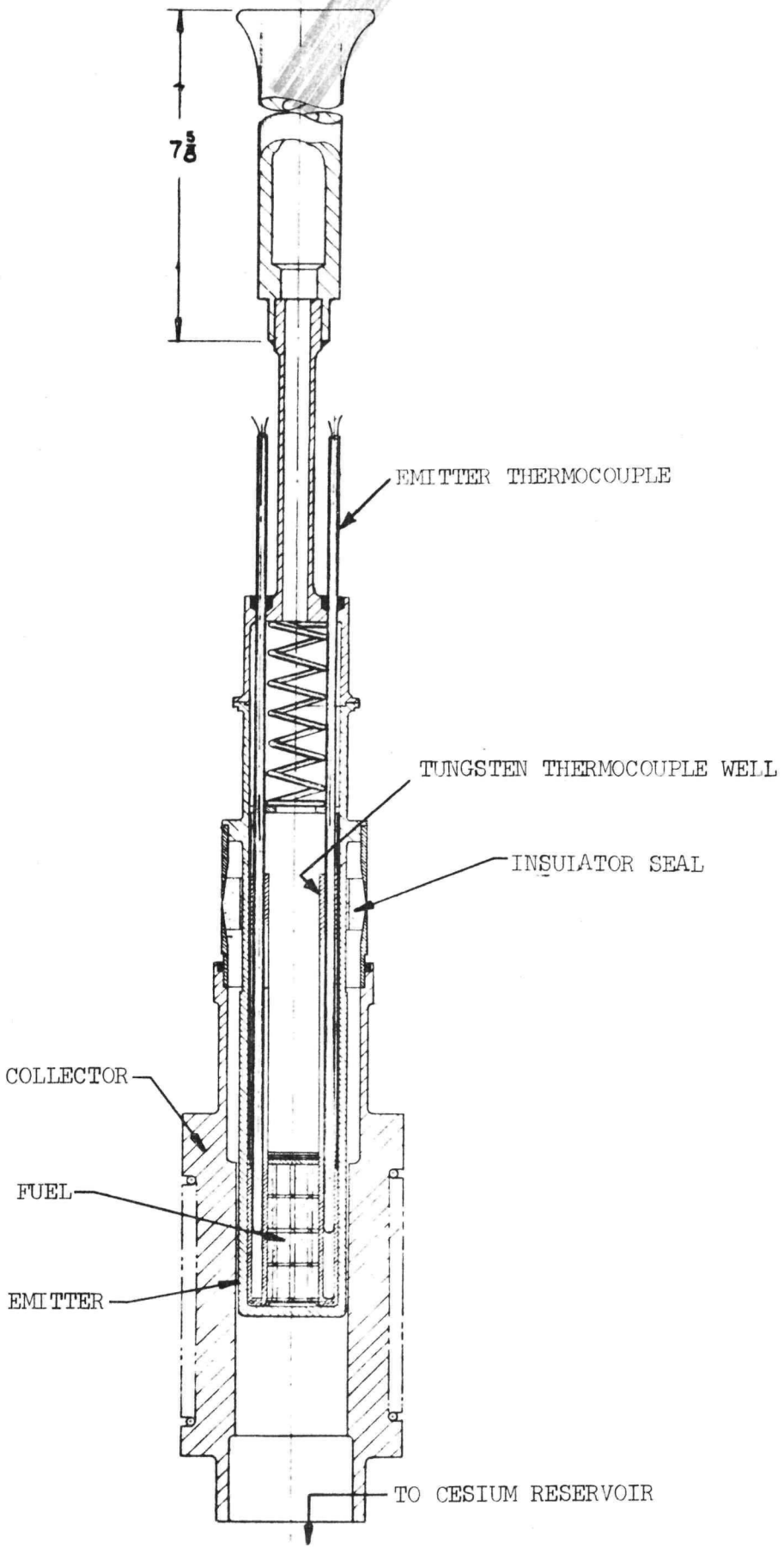

Fig. 1. Schematic arrangement of components in Converter IC-I3

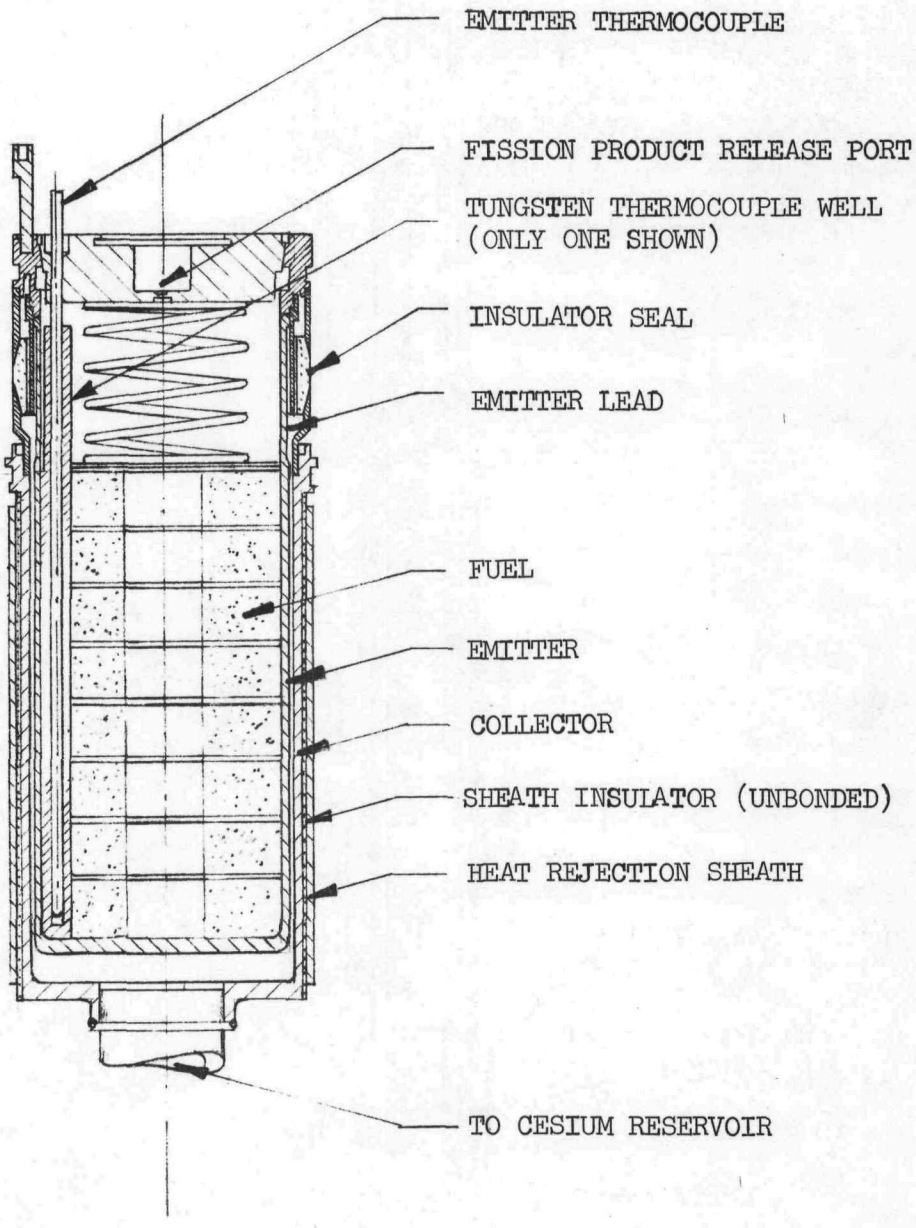

Fig. 2. Schematic arrangement of components in Converter IC-C3

CONVERTER IC-I3

The primary containment of Converter IC-I3 was punctured in an enclosed chamber in the hot cell and the gas collected in a charcoal trap was counted for its Kr^{85} content. On the basis of the radiochemical counting result and the fission power input to the emitter during in-pile operation, it was estimated that about 65% of the fission gas atoms formed was released from the fuel.

When the converter was removed from the primary containment, it was found that one of the cesium reservoir heaters was burned out (Fig. 3). A black film was observed over the surface of the top of the fission product chamber and the Al_2O_3 insulator around it. The lower part of the BeO insulator for the high temperature thermocouple was also covered by a black film of similar nature. It appears that leaks have developed either in the braze of the W-25Re thermocouple sheath to the tantalum transition piece of the emitter or in the W-25Re sheath itself, and that the black film was formed by the condensation of materials transported from the fuel chamber through these leaks by vaporization. It was probably through these leaks that the fission gas in the fission product chamber entered the primary containment of the converter.

When the emitter was removed from the collector, a longitudinal crack was found over the fueled region, directly above one of the thermocouple wells. The tungsten cladding was otherwise intact. Figure 4 shows the emitter assembly and Fig. 5 shows the position of the crack relative to that of the thermocouple well. The crack seems to be originated from stress concentration on the cladding due to the presence of the thermocouple well. This became more evident when the microstructures of the cladding in contact with the thermocouple well were examined under a microscope (see below). Very likely it was through this crack that the argon gas in the primary containment entered the interelectrode space by way of the fission product and fuel chamber.

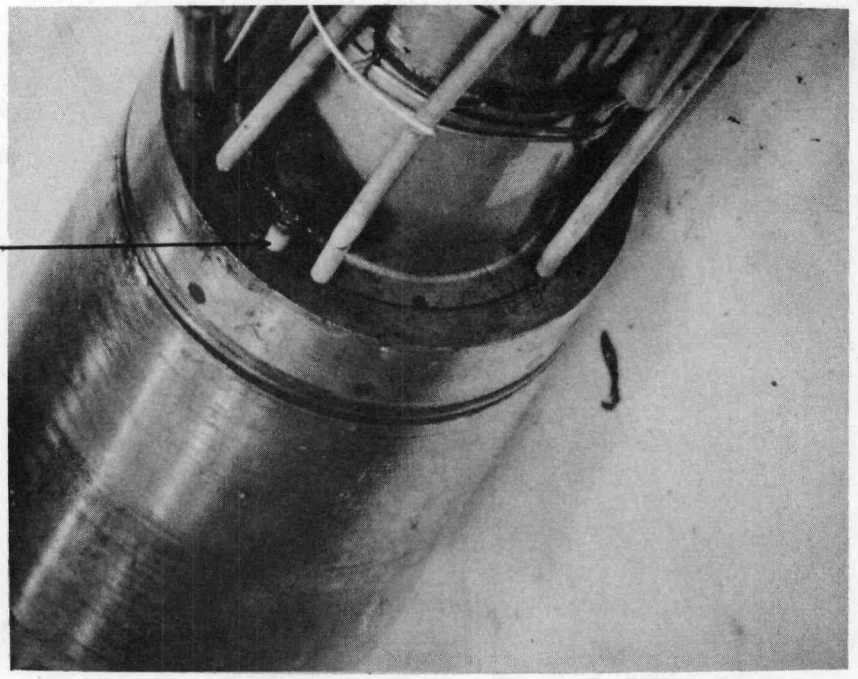

Fig. 3. IC-I3 collector top, showing the burn-out of one of the cesium reservoir heater wire

18

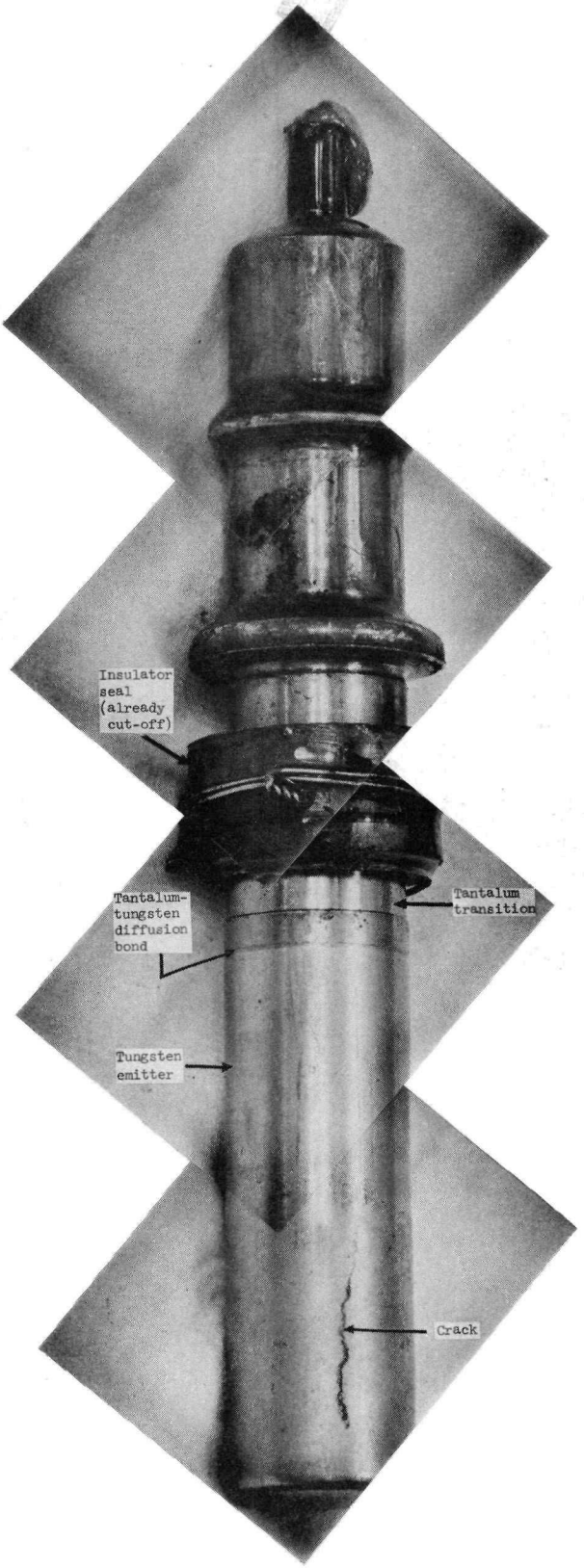

Fig. 4. Emitter assembly of IC-I3

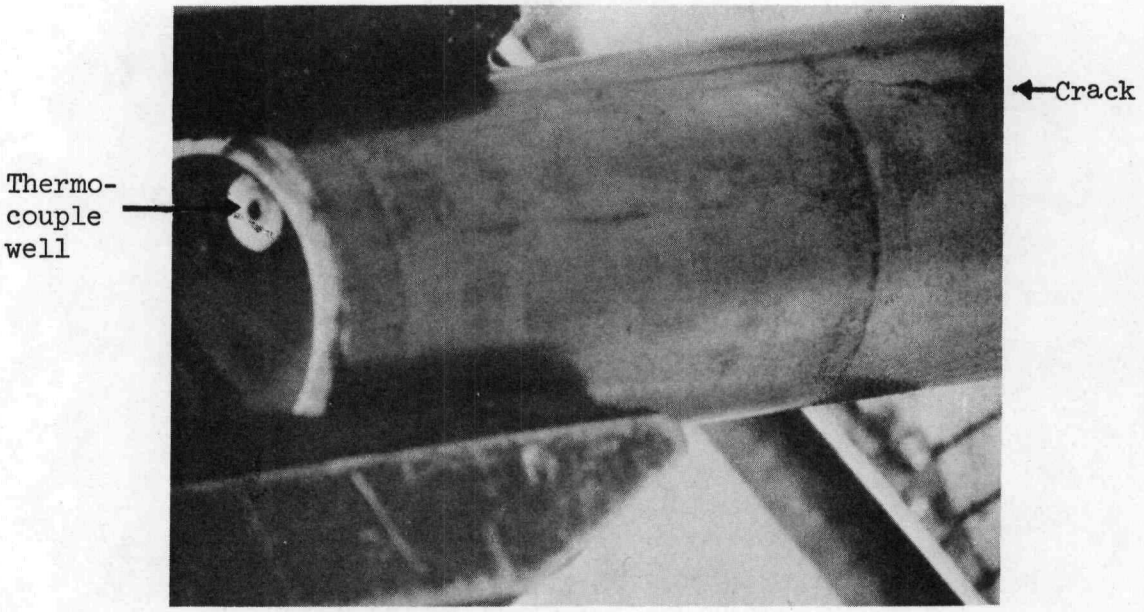

Fig. 5. IC-I3 emitter cut off from emitter stem, showing that the crack is located over the thermocouple well

Table 2 shows the dimensions of the emitter measured at different axial and azimuthal positions. It appears that the maximum change in emitter dimension is located over the crack, which amounts to a radial expansion of about 2 mils.

Figure 6 shows a longitudinal cross section of the fueled emitter at 7X magnification. It can be seen that there exists a reaction layer over all the fuel-tungsten interface. The thickness of the layer is less near the top of the emitter, where the temperature is lower. Figure 7 is a magnified view (20X) of the top region of Fig. 6, showing the reduction in the thickness of the tungsten cladding due to this interaction. Measurements made of the thickness of the reaction layer and that of the tungsten cladding at various axial locations indicate that the maximum thickness of this reaction layer is about 10 mils and the maximum loss of the thickness of the tungsten cladding is about 5 mils, i.e. about 10% of the original thickness of the cladding was lost in 7343 hours. The reaction product has a dense columnar grain structure, as shown in Fig. 8.

Figure 9 shows the structures of the fuel-material near the fuel-cladding interace and that near the center region of the fuel. There does not appear to be any major difference in the pore structures of these two locations.

Figure 10 shows a transversal section of one half of the fueled emitter. Cracks can be seen in the thermocouple well at a number of places. The relative position of the crack in the tungsten cladding to that in the thermocouple well is apparent. The small venting holes (16 holes of 0.025 inch diameter) have disappeared because of fuel swelling. As shown in Fig. 6, a good part of the central venting channel has also vanished because of the same reason. The total amount of the change in the volume of the fuel body including axial extrusion and the loss of the venting holes and part of the central venting channel, is estimated to be about 10%.

TABLE 2

DIAMETERS OF TUNGSTEN EMITTER OF CONVERTER IC-I3
AFTER IN-PILE OPERATION

(As fabricated emitter diameter = 0.6460 inch)

Axial Location (Inch From Closed End Emitter Bottom)	Azimuthal Positions (See Attached Figure)		
	1-1	2-2	3-3
1/8"	0.6498	0.6492	0.6493
1/4"	0.6503	0.6498	0.6494
1/2"	0.6508	0.6495	0.6499
3/4"	0.6498	0.6492	0.6495
1"	0.6497	0.6487	0.6487

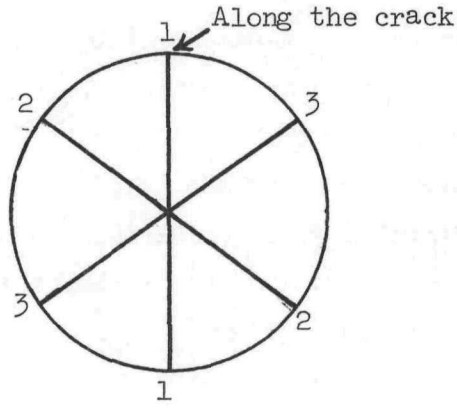

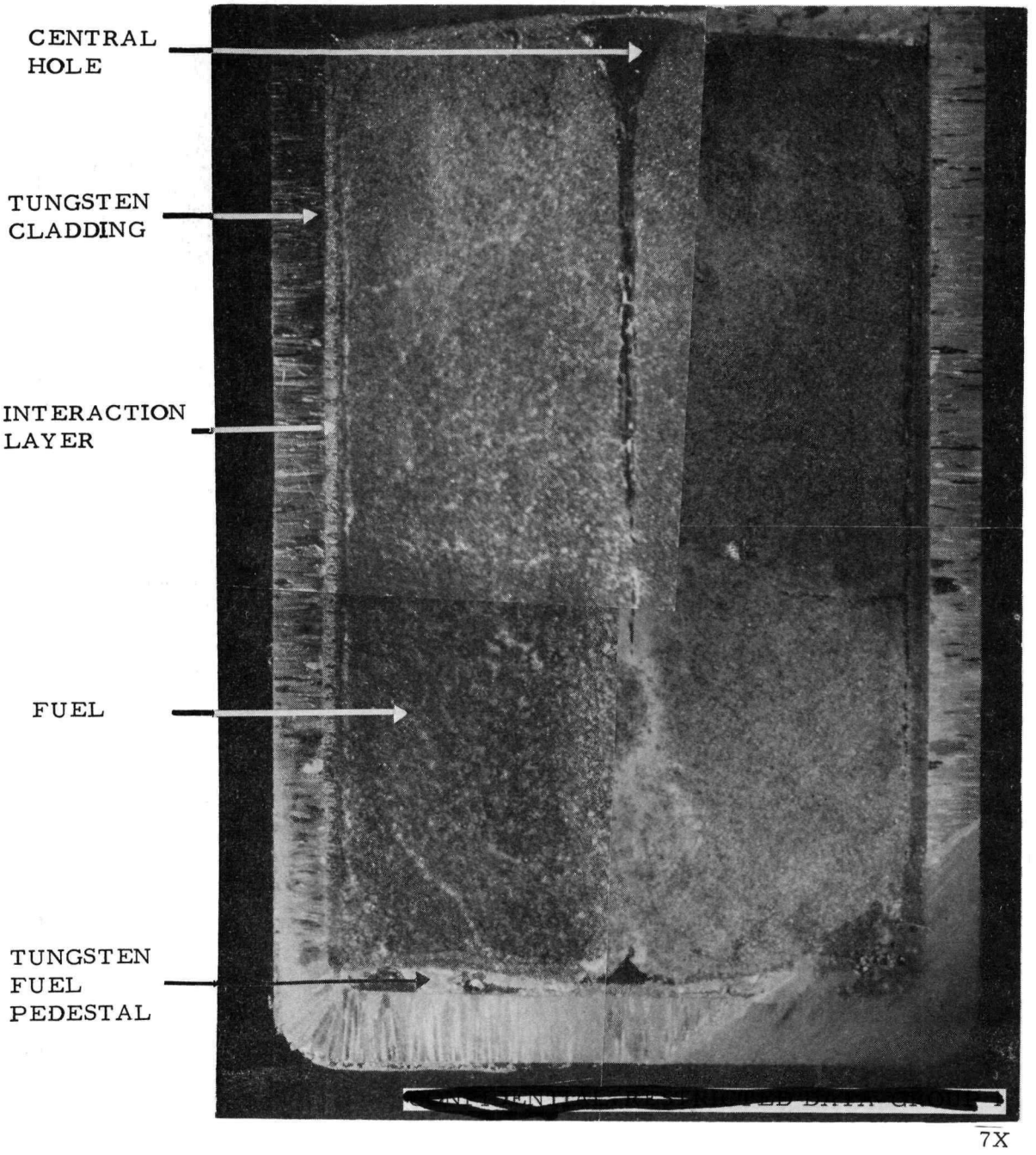

Fig. 6. Cross section view of the fueled emitter of converter IC-I3

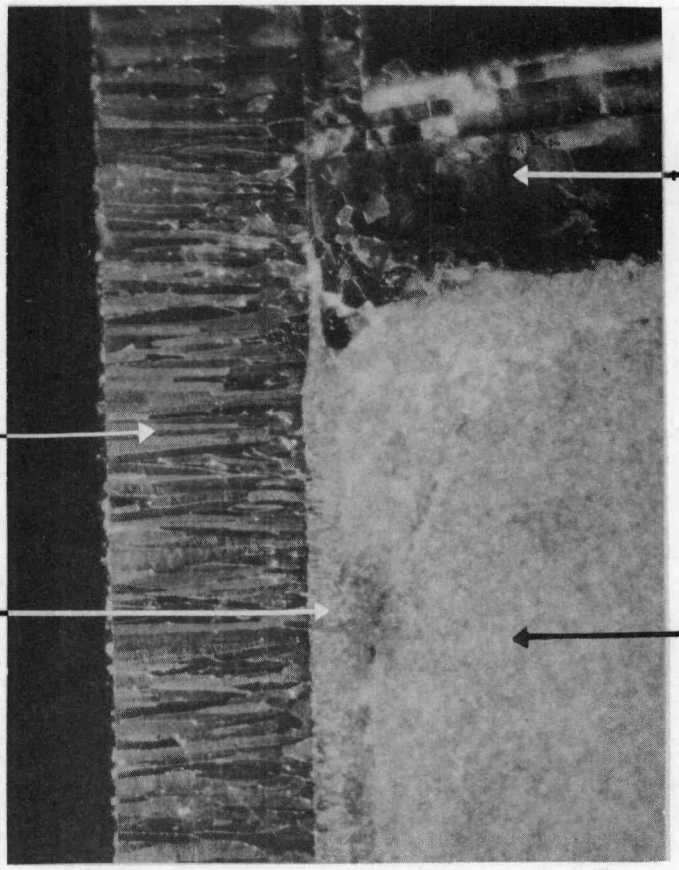

Fig. 7. Magnified view of the top left corner of Fig. 4

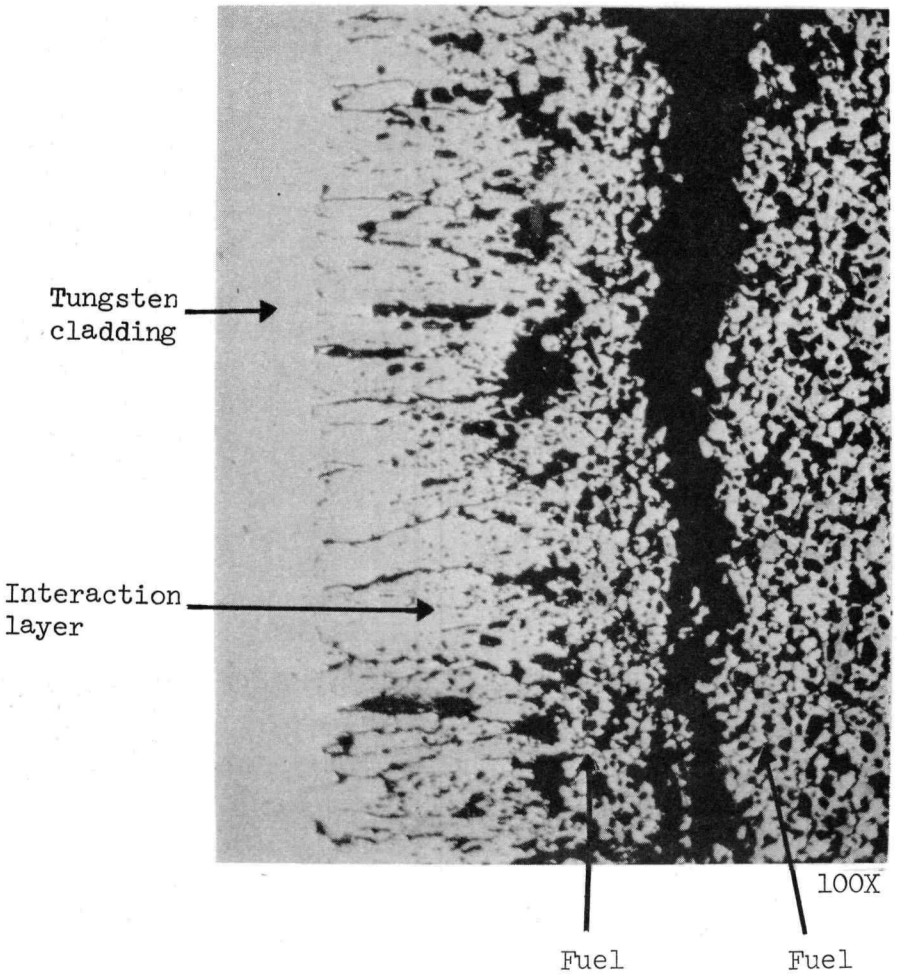

Fig. 8. Columnar structure of the reaction layer at the fuel-cladding interface (100X)

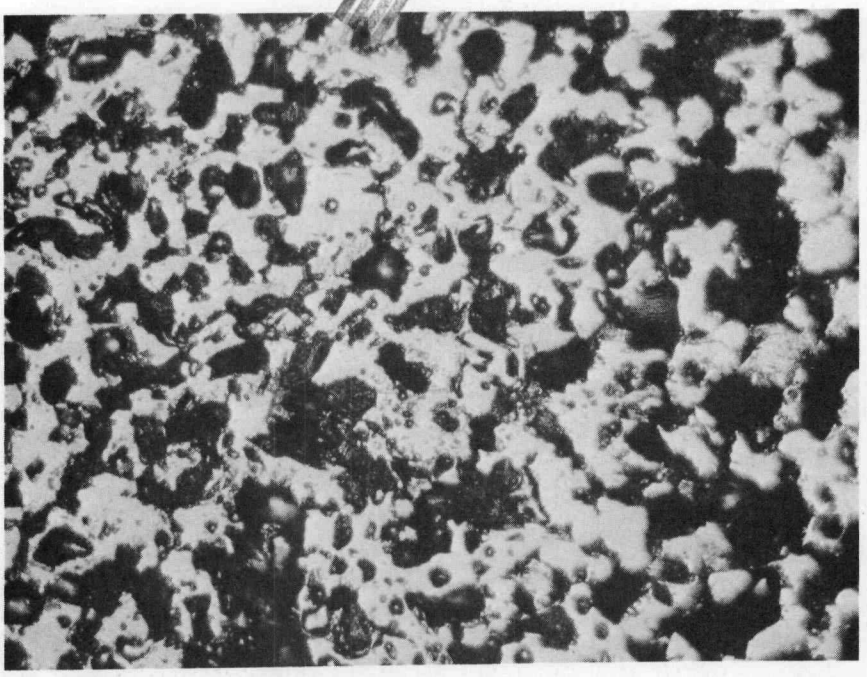

250X

(a) Near fuel-cladding interface

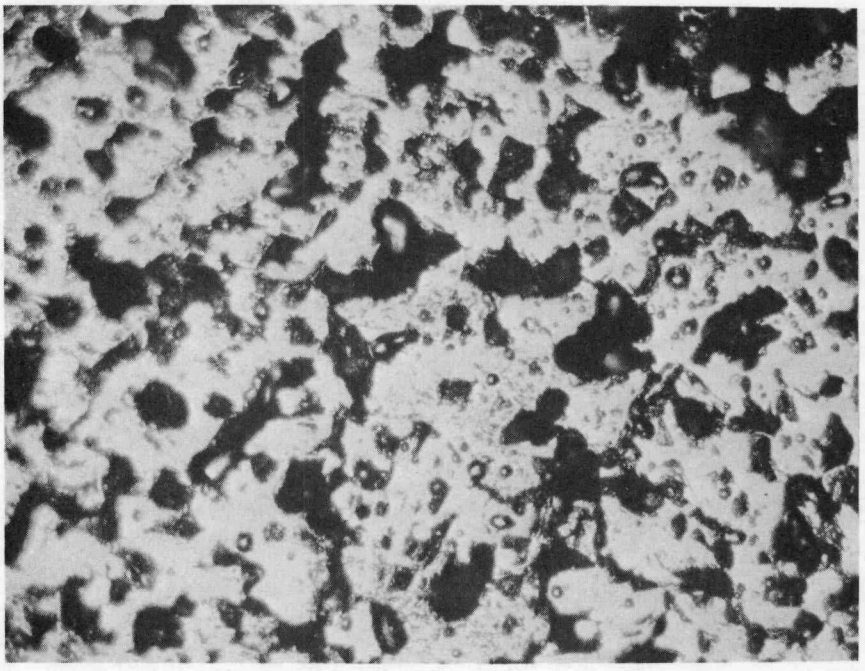

250X

(b) Near center of fuel

Fig. 9. Structures of the fuel material in Converter IC-I3 (250X)

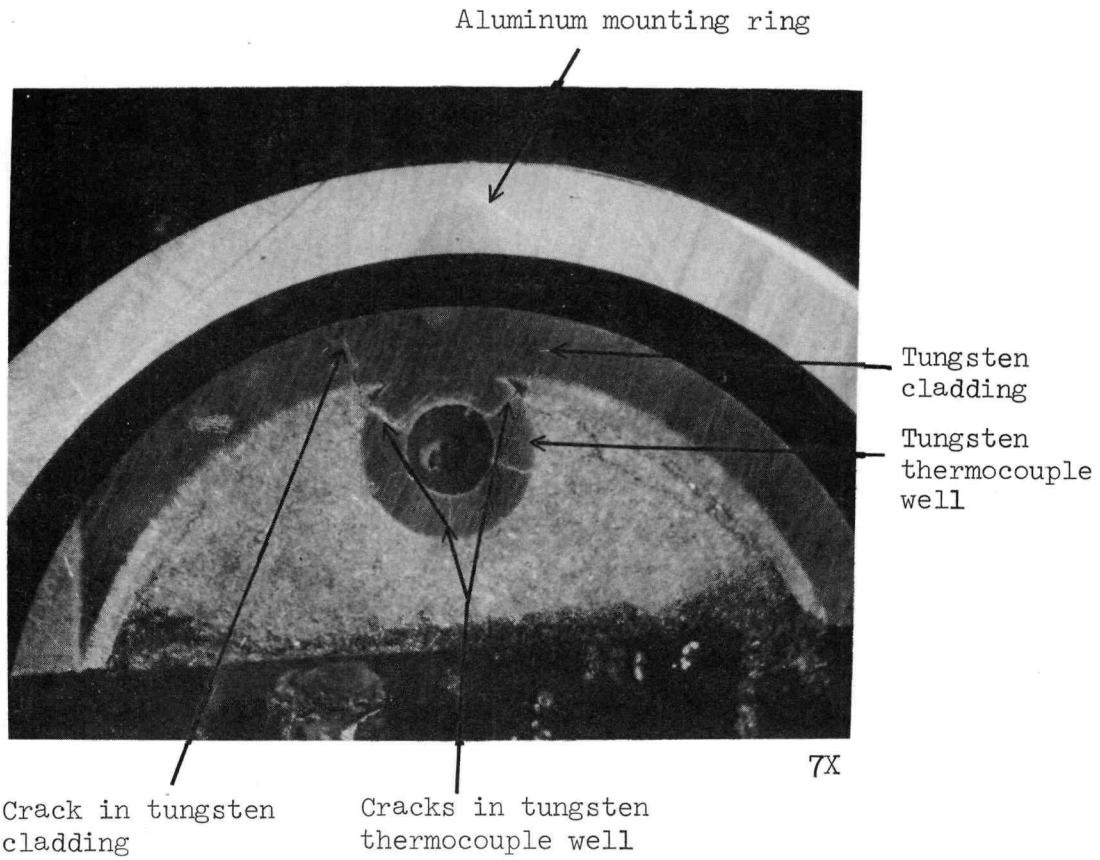

Fig. 10. Transversal section of one half of the fueled-emitter of Converter IC-I3

More detailed metallography and electron microprobe analysis of the sample shown in Fig. 10 were carried out at Battelle Memorial Institute* where hot cell examinations of similar type of fuel-cladding system were made about one and one half years ago. Figure 11 shows this sample at 20X magnification. The areas A, B, and C where electron microprobe analyses were made are indicated on the figure. The diamond shaped marks are the indentations made during microhardness measurements. The tungsten cladding, the tungsten thermocouple well and the fuel-cladding interaction layer are shown in the figure, but most of the fuel material was lost during polishing. A small amount, however, is still left (area C in Fig. 11) to allow metallographic and electron microprobe examinations to be made on the fuel for comparison with the metallographic results shown in Figs. 8 and 9.

One of the distinctive features shown in Fig. 11 is the microstructures of the cladding and that of the thermocouple well in the vicinity of the cracks observed in the cladding. An enlarged version of this region is shown in Fig. 12. The thermocouple well was not bonded to the inner surface of the cladding when the converter was assembled, although the contacting surfaces were machined to insure good fit. This interface, however, seems to have disappeared in Fig. 12. Grain growth has occurred in the vicinity of the contact area to bridge over the interface. It is believed that a force, probably produced by fuel swelling, has pushed the thermocouple well against the inner surface of the cladding and the stress generated has induced grain growth and led to the diffusion bonding of thermocouple well to the cladding. The growth of the grains undoubtedly has swept impurities to the grain boundaries to weaken the structures there. Since the force is concentrated to a small contact area, much like the drive of a blunt-ended wedge, the high stress concentration, especially upon thermal cycling, produced cracks along the grain boundaries. Microhardness measurements were made in the areas near the cracks in the cladding and the thermocouple well, which are indicated by letters in Fig. 12. The results are shown in Table 3.

---

*The help of Victor Storhok, Richard Hilbert and Vincent Scotti are gratefully acknowledged.

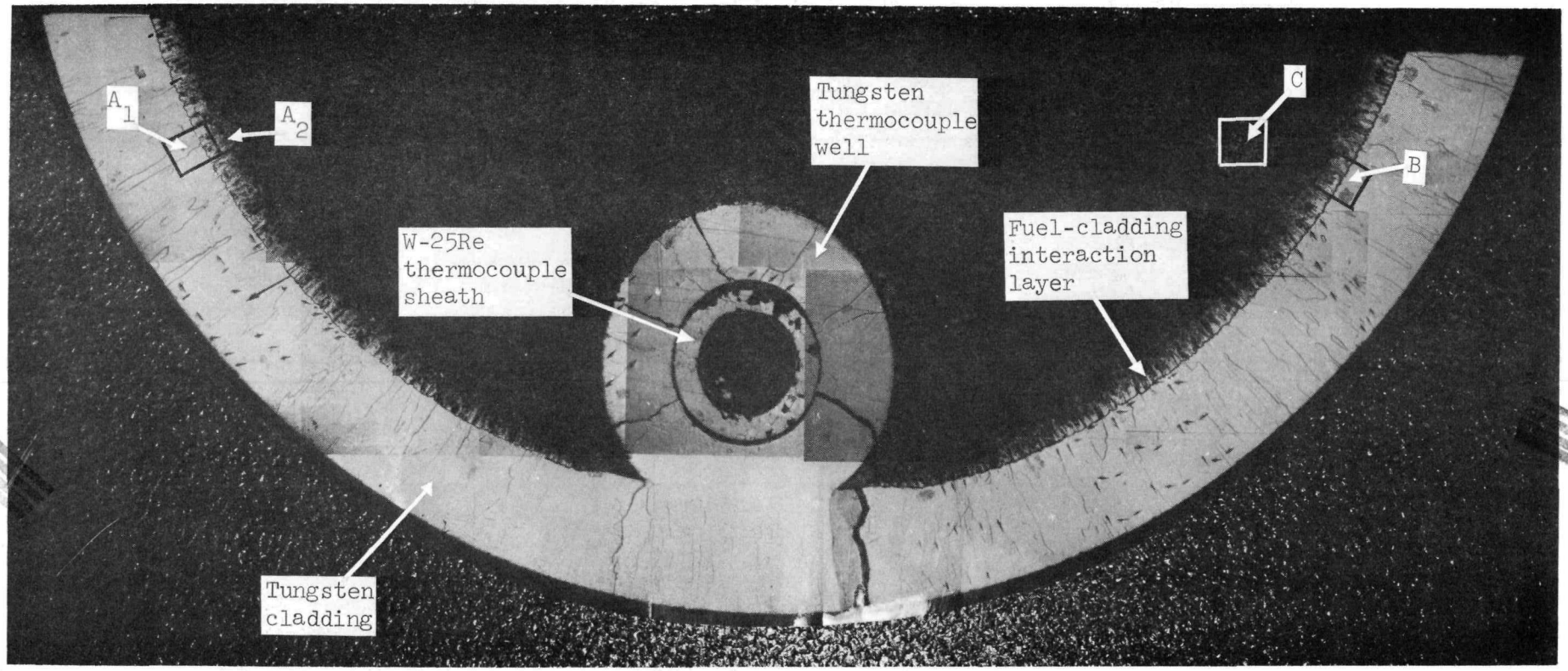

Fig. 11. Composite microstructure of sample sent to BMI for metallography and electron microprobe examinations. A_1, A_2, B and C are the areas where electron microprobe analyses were carried out. The indentations are marks made during microhardness measurements

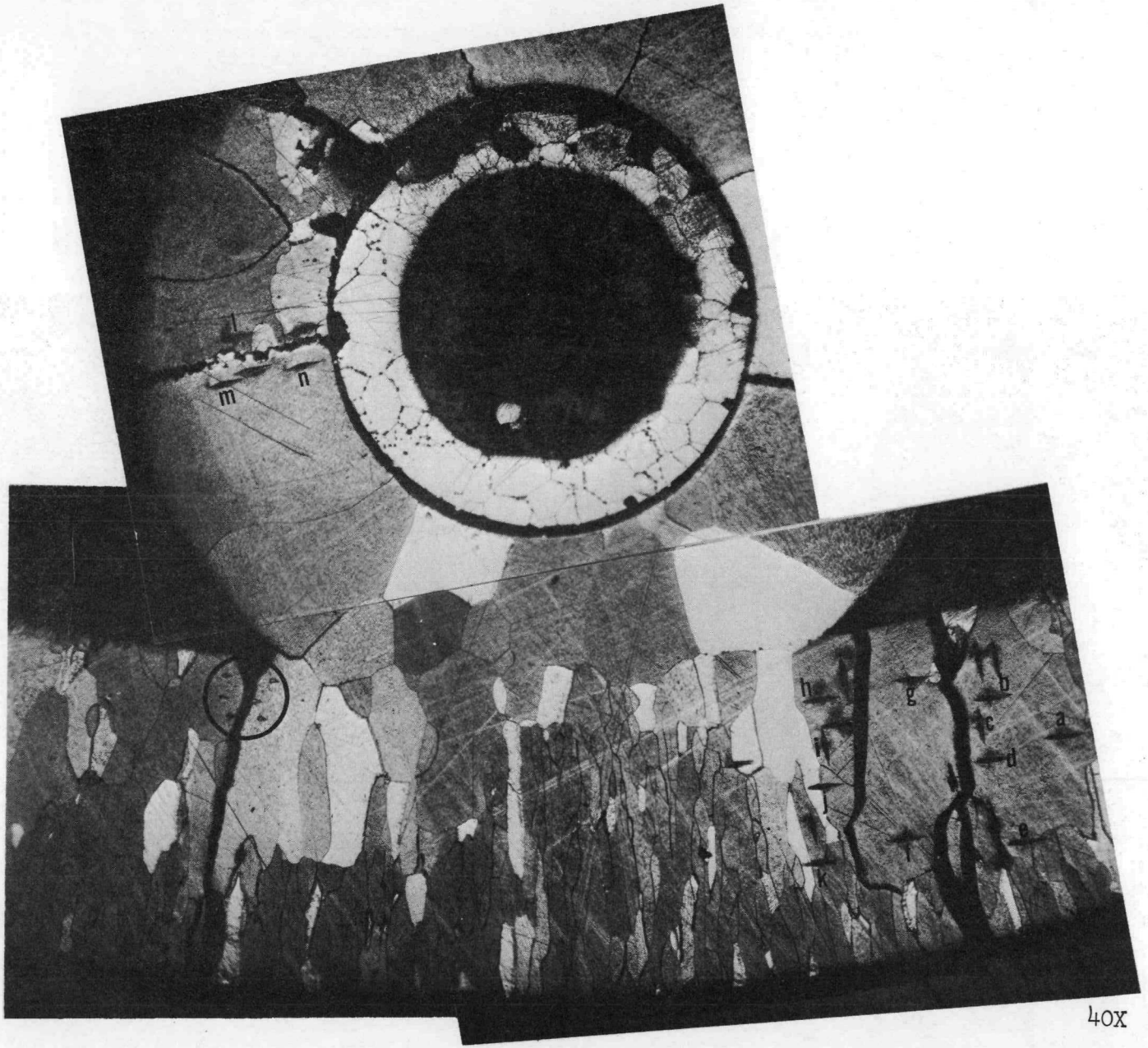

Fig. 12. Etched microstructure of the tungsten cladding and thermocouple well near the region where cracks occurred in the cladding. The letters indicate areas where microhardness measurements have been made

CONFIDENTIAL

TABLE 3

MICROHARDNESS DATA TAKEN NEAR CRACKS
IN CLADDING AND THERMOCOUPLE WELL

Indentation (see Fig.12)	Knoop Hardness Number (500 gm load)
a	358
b	341
c	320
d	329
e	314
f	350
g	322
h	348
i	332
j	355
k	408
l	300
m	322
n	325

These values are similar to the hardness of unirradiated fluoride tungsten. In addition to the measurements using 500 gram load, measurements were also made very close to one of the cracks in the cladding at 25 gram load (the area encircled in Fig. 12). The results show no increase in hardness. Perhaps the embrittlement of the grain boundaries is very local in nature and the microhardness measurements are not "fine" enough to detect it. Microhardness measurements were also made in regions away from the cracks. Figure 13 shows one of such regions. The results obtained are shown in Table 4. The cladding seems to be harder upon approaching the outer edge and when the indentation is oriented perpendicular to the elongated grains. The difference, however, is small. Data taken at several other areas of the cladding are consistent with the data shown in Table 4. There is no significant difference between these data and the hardness of unirradiated fluoride tungsten.

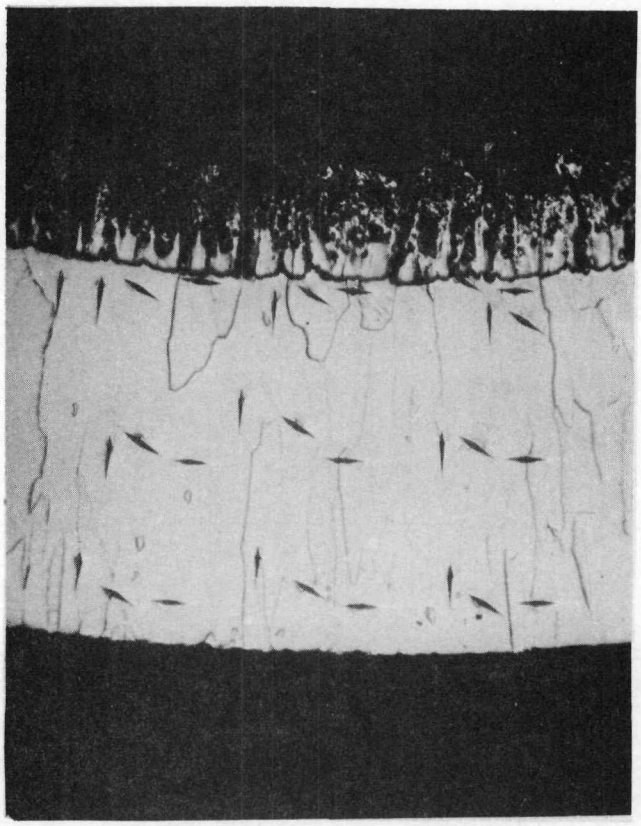

40X

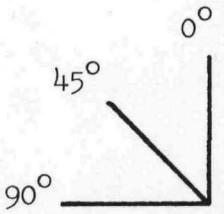

Fig. 13. Photomicrograph of the area where the hardness data given in Table 4 were obtained

TABLE 4

MICROHARDNESS DATA FROM THE TUNGSTEN CLADDING

Orientation of Indentation	Knoop Hardness Number (500 gm load) Position of Measurement		
	Inside Edge	Center	Outside Edge
0°	281.80	308.67	331.10
45°	324.38	306.27	355.17
90°	330.82	369.10	391.25
Average	312.33	328.01	359.17

Typical microstructures of the cladding are shown in Figs. 14(a) and (b). No grain boundary porosity can be detected. The width of the columnar grains range from 50 to about 500 microns. The majority of the grains have a width of about 80 microns.

Figures 15(a) and (b) illustrate the microstructures of the fuel-cladding interaction layer, which are similar to that shown in Fig. 8. The reaction layer has a columnar grain structure and the interface between the layer and the cladding is uneven when viewed at high magnification (see Fig. 15(a)). There is a second phase of light colored particles in the columnar grain (see Fig. 15(a) and near the inner edge of the interaction layer (see Fig. 15(b)). The areas A_1 and B at the interaction layer-cladding interface (see Fig. 11) and the area A_2 at the inner edge of the interaction layer (see Fig. 11) were analyzed by electron microprobe. Figures 16(a) and (b) are the uranium and the tungsten scans* respectively for area A_1 at the interaction layer-cladding interface. It can be seen that the interaction layer consists of a matrix containing uranium and tungsten and some dispersions of a tungsten-rich (uranium-poor) phase and that the tungsten cladding contains virtually no uranium. Similar conclusions can

*All electron microprobe scanning pictures in this report have a magnification of 430X.

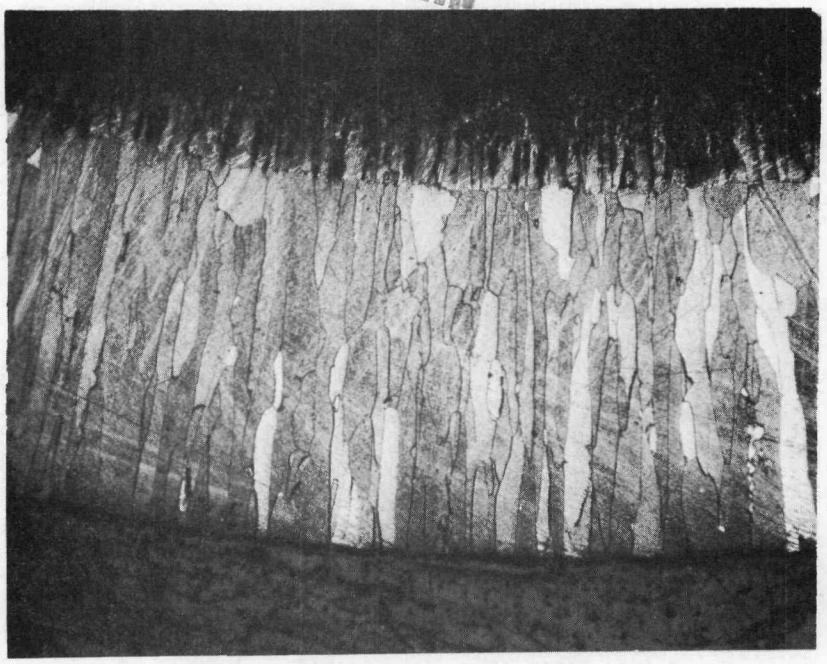

40X

(a) No grain growth

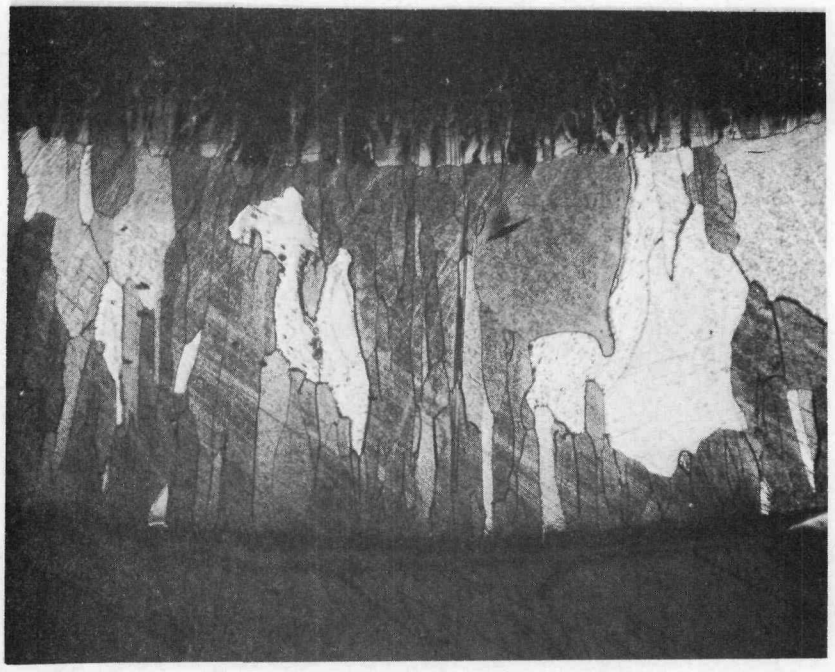

40X

(b) Some grain growth

Fig. 14. Etched microstructure of the tungsten cladding

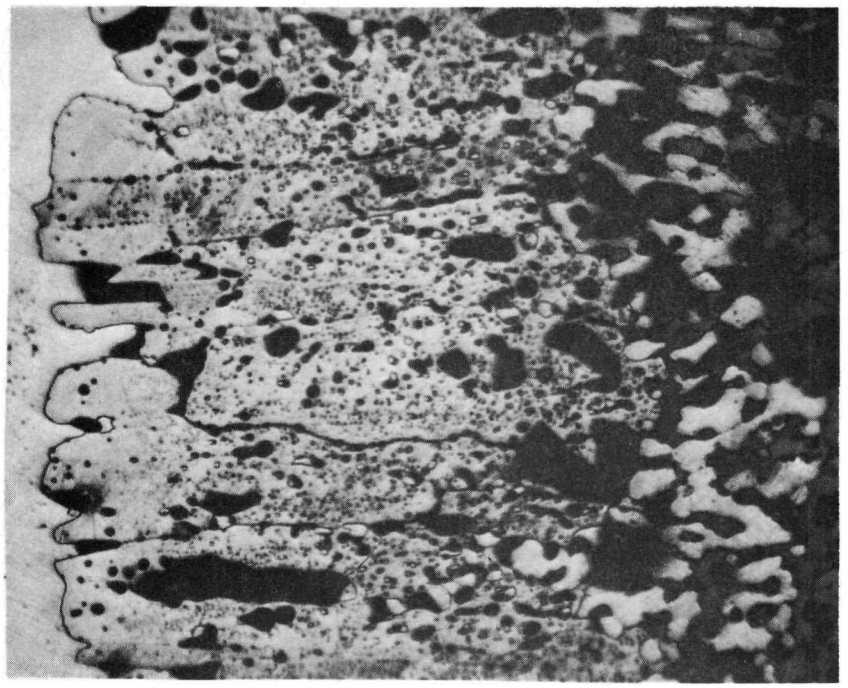

250X

(a) Note that there is a second phase of very fine, light-colored particles in the columnar grain of the interation layer

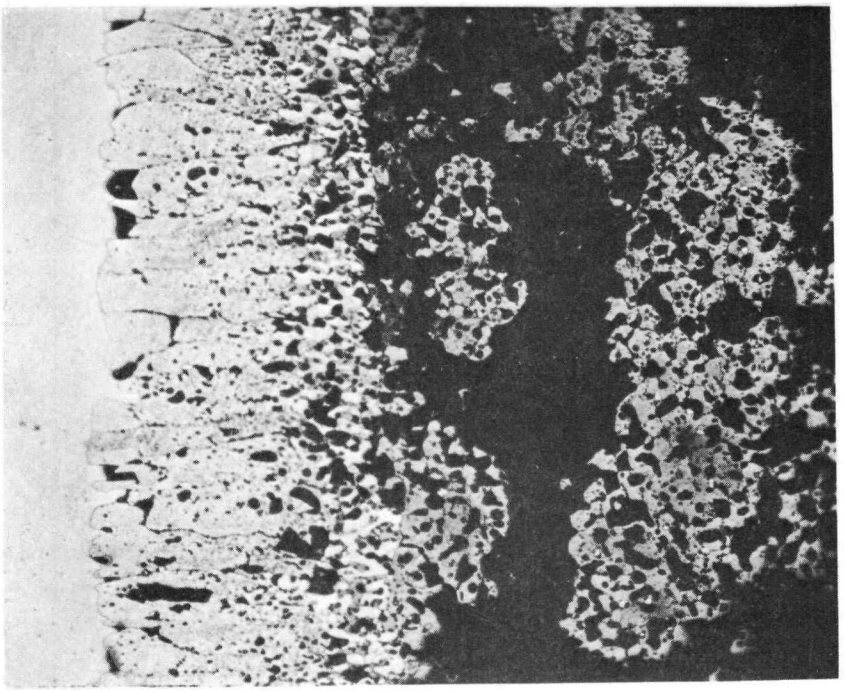

100X

(b) Note the light-colored phase at the inside edge of the fuel-clad interation layer

Fig. 15. Photomicrographs of the fuel-clad interaction layer

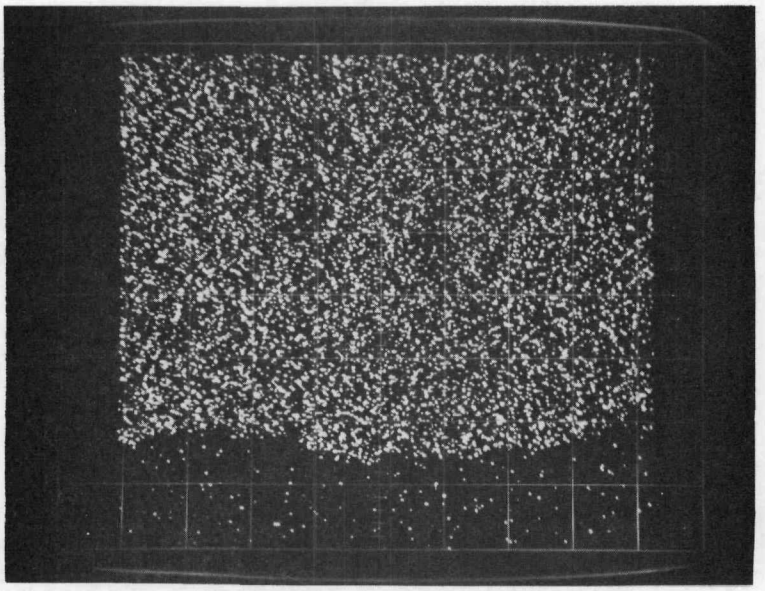

(a) Uranium $M_{\alpha 1}$ scan

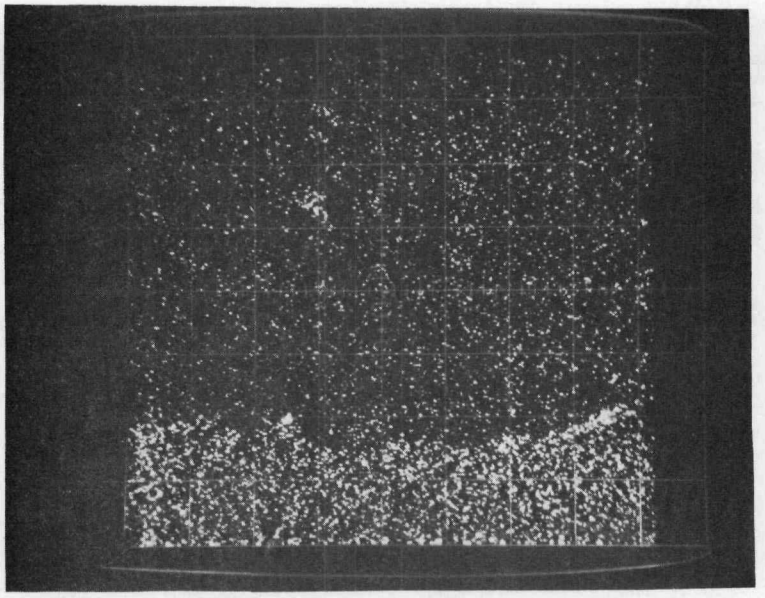

(b) Tungsten $L_{\alpha 1}$ scan

Fig. 16. Electron microprobe analysis of area A_1 at the interaction layer-cladding interface

be drawn from Figs. 17(a) and (b) which are respectively the uranium and the tungsten scans for area B at the interaction layer-cladding interface. Some tungsten "fingers" can be seen extending from the cladding into the interaction layer, indicating non-uniform interaction at the interface. The high intensity of the "tungsten fingers" which suggests a tungsten concentration greater than that of the cladding, is a result of the beam traversing the extremely rough surface of the sample. Figures 18(a) and (b) are the uranium and the tungsten scans respectively for area A_2 at the inner edge of the fuel-cladding interaction layer. It can be seen that the light-colored second phase observed in Fig. 15 at the inner edge of the fuel-cladding interaction layer is highly rich in tungsten and may contain a small amount of uranium. To determine quantitatively the uranium, tungsten and zirconium contents in the interaction layer, the X-ray intensities were measured at several areas by point counting techniques and the raw data obtained were corrected for dead-time, background, absorption and atomic number by a computer program, which has been shown to be accurate to within 4 percent for concentrations greater than 10 weight percent. The average uranium and tungsten concentrations in the interaction layer were found to be 53 weight percent and 38 weight percent respectively. Variations of uranium concentration from 39 weight percent to 64 weight percent and tungsten concentrations from 21 weight percent to 63 weight percent have been observed. However, the ranges given represent only the extremes. In fact, there was little variation in uranium and tungsten concentrations across the interaction layer and most of the concentration data were close to the average values. The zirconium concentration varied from 0 to 1 weight percent. However, due to the very large corrections applied to the zirconium data, the best can be said is that zirconium was detected in the interaction layer. Thus the interaction layer can be considered as containing 53 weight percent uranium and 38 weight percent tungsten. These values agree fairly well with the uranium and zirconium concentrations of UWC_2 (53 weight percent uranium and 41 weight percent tungsten), a mixed carbide phase which is known to exist for the U, W, and C ternary system. The UWC_2 interaction layer was probably formed by the carburization of the tungsten from the cladding, followed by the alloying of the tungsten carbide formed with the UC in the carbide fuel. The exact mechanism through which the reaction occurred is

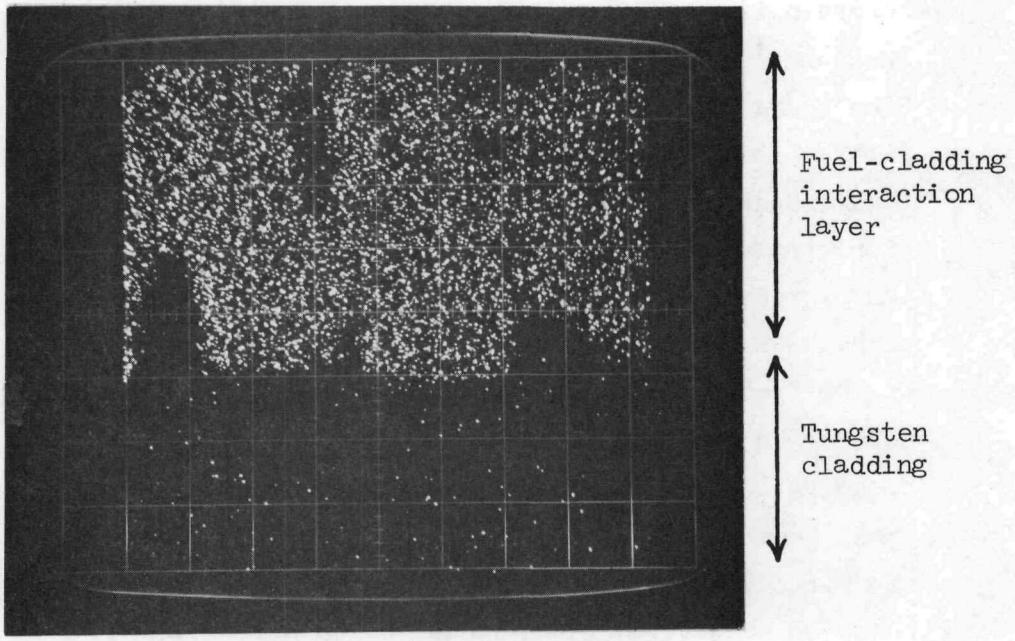

(a) Uranium $M_{\alpha 1}$ scan

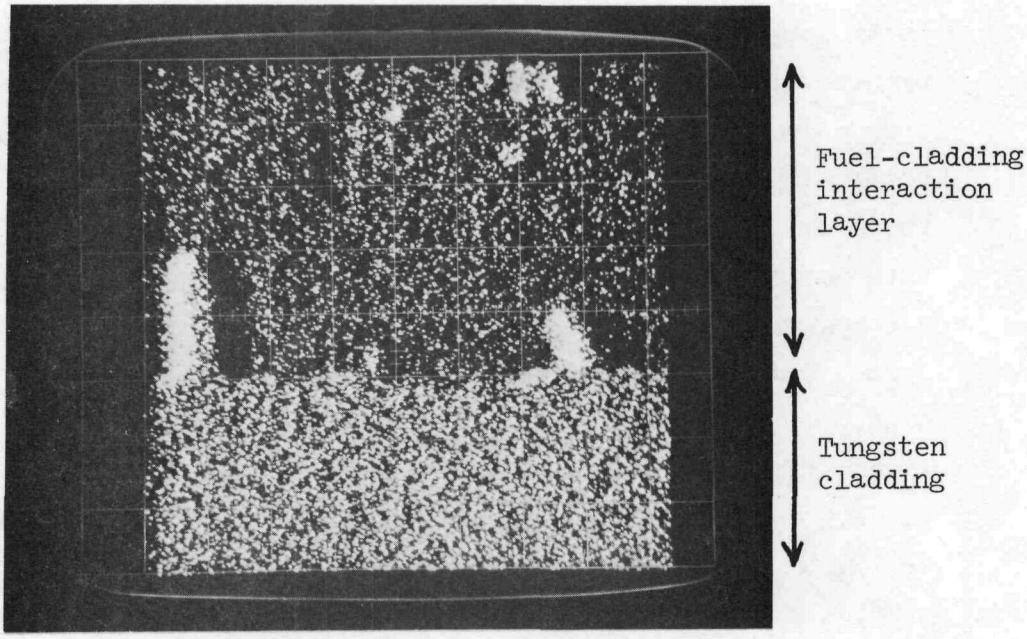

(b) Tungsten $L_{\alpha 1}$ scan

Fig. 17. Electron microprobe analysis of area B at the interaction layer-cladding interface

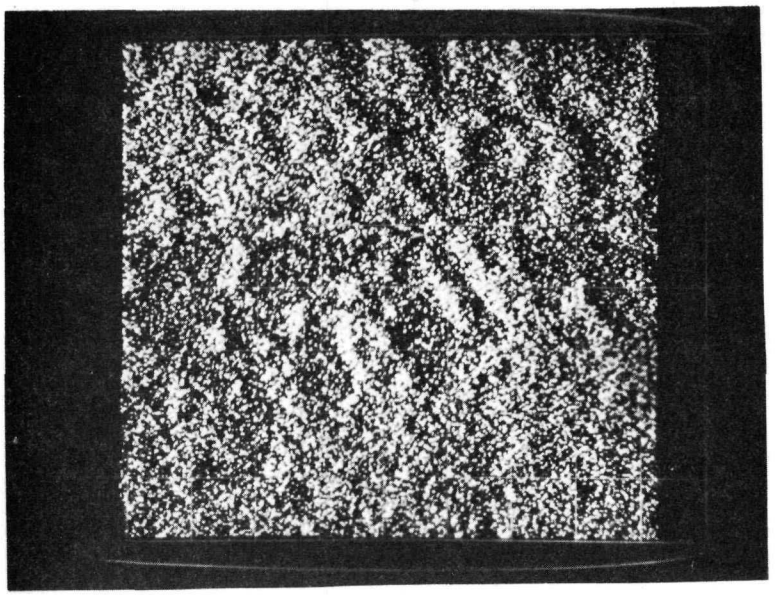

(a) Uranium $M_{\alpha 1}$ scan

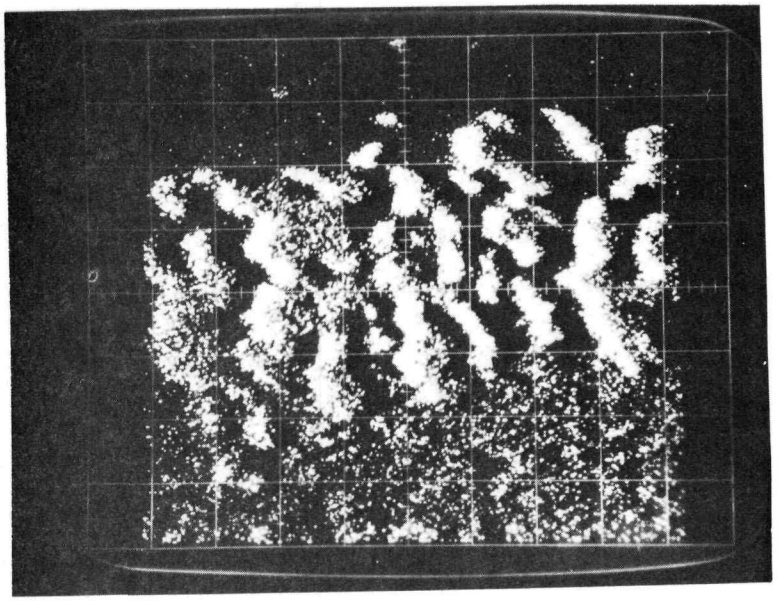

(b) Tungsten $L_{\alpha 1}$ scan

Fig. 18. Electron microprobe analysis of area A_2 near the inner edge of the fuel-cladding interaction layer

not clear. However, judging from the fact that a tungsten rich phase (probably tungsten carbide) was found at the junction between the UWC_2 phase and the carbide fuel, it seems that the carburization and the alloying occurred mostly at the interface between the interaction layer and the fuel, with the tungsten arriving at this interface from the cladding through a tungsten gradient in the UWC_2 phase. Since UWC_2 phase has a finite stoichiometry range, it is entirely conceivable that the tungsten concentration is slightly higher when in contact with the tungsten cladding than when in contact with the carbide fuel, although the difference maybe too small to be measured by electron microprobe analysis. Out-of-pile study of the compatibility between tungsten-containing 90UC-10ZrC of C/U = 1.05 (same as the C/U ratio of the fuel of Converter IC-I3) and tungsten under isothermal condition at 1800°C for 100 hours showed no interaction. It is possible that the testing time was not long enough to allow any appreciable interaction. It is also possible that although no reaction was observed under isothermal conditions, the presence of a temperature gradient in the fission heated fuel body may induce carbon migration toward the fuel-cladding interface to raise the carbon activity there to a value exceeding the limit for fuel-cladding compatibility. These are the areas where carefully planned work is needed to help to elucidate the mechanism of the interaction between tungsten and carbide fuel materials.

Figure 19 is a photomicrograph of the fuel material taken of the area C in Fig. 11. Electron microprobe analysis indicates the presence of about a few weight percent of dissolved tungsten. The light-colored dispersion consists of tungsten-rich phases, presumably W and UWC_2. The microstructure is similar to that observed in out-of-pile metallographic study of such carbide fuel material, except that the irradiated fuel material contains a large number of fission gas bubbles in the grains of the matrix.

Figures 20 and 21 show respectively the macroscopic appearance and the microstructures of the interface between the tantalum transition piece and the tungsten emitter stem. It is estimated that the diffusion bond operated in the temperature range 1200-1300°C. The bond seems to remain intact, although some Kirkendall voids are present on the tantalum side of the

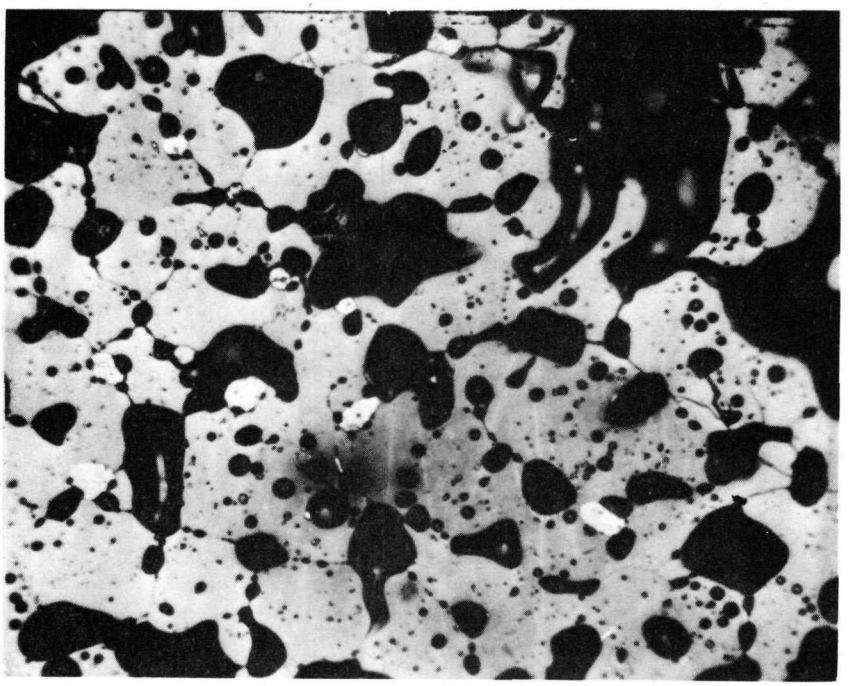

500X

Fig. 19. Microstructures of the carbide fuel material in area C of Fig. 11

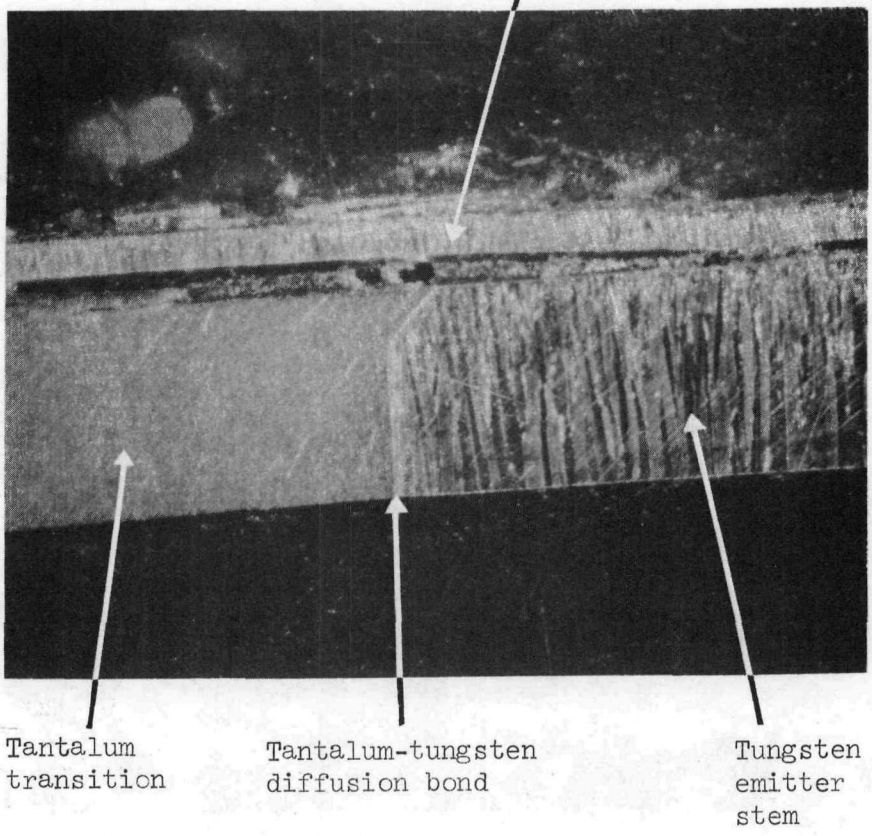

Fig. 20. Post-irradiation appearance of the Ta-W diffusion bond in Converter IC-I3 (20X)

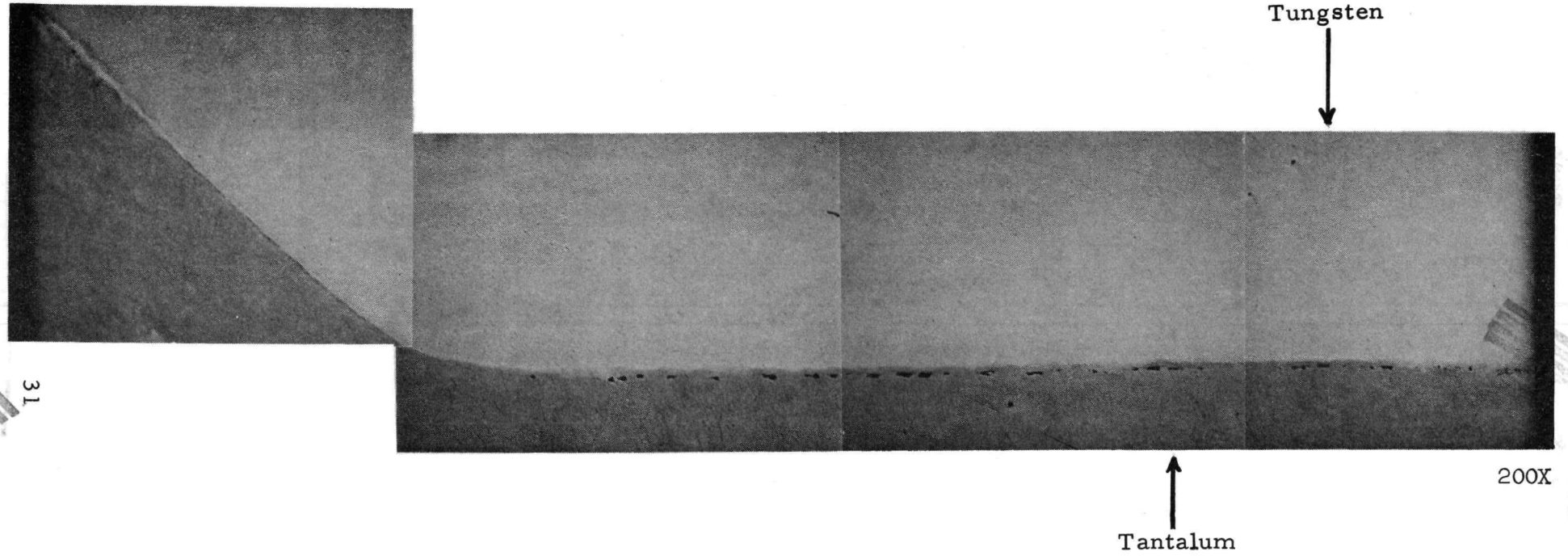

Fig. 21. Appearance of the tantalum-tungsten diffusion bond interface in Converter IC-I3

interface. The results indicate no serious problem associated with the use of the tantalum-tungsten bond in the design of the thermionic fuel element.

CONVERTER IC-C3

Figure 22 shows the converter assembly after its removal from the primary containment. The exterior surfaces of all the components were clean, except that some black films were present around the brazed joint between the high temperature thermocouple sheath and the tantalum transition piece, probably due to the vaporization of materials from the fuel chamber through leakage at the braze or in the W-25Re thermocouple sheath. A large amount of fission gas was detected when the primary containment was cut open, indicating that the puncturing device has properly functioned and that the fuel chamber was in communication with the primary containment.

The graphite sorption reservoir was cut off from the converter assembly and the unbonded sheath insulator was removed. The insulator seal-tantalum transition assembly was then separated from the emitter-collector assembly at a point slightly above the final closure braze by cutting with a SiC disc. The cutting path passed between the top of the fuel body and the first tungsten radiation shield. Figure 23 shows the appearance of the top of the fuel body. It can be seen that the top of the central venting channel remained open, although it became tapered further down into the cavity because of fuel swelling. The indentation marks on the central portion of the top of the fuel were formed when the fuel was pushed against the tungsten radiation shield by the swelling. This is borne out by the appearance of the surface of the radiation shield where similar indentations are evident, (Fig. 24). Figure 25 represents a view of the bottom of the emitter, where cracks were found.

The emitter looked clean when removed from the collector. A point where the emitter was shorted to the collector was found at a location about 1/4 inch from the bottom of the emitter (Fig. 26). Such a partial short was noticed during the test of this converter. It is believed that this partial

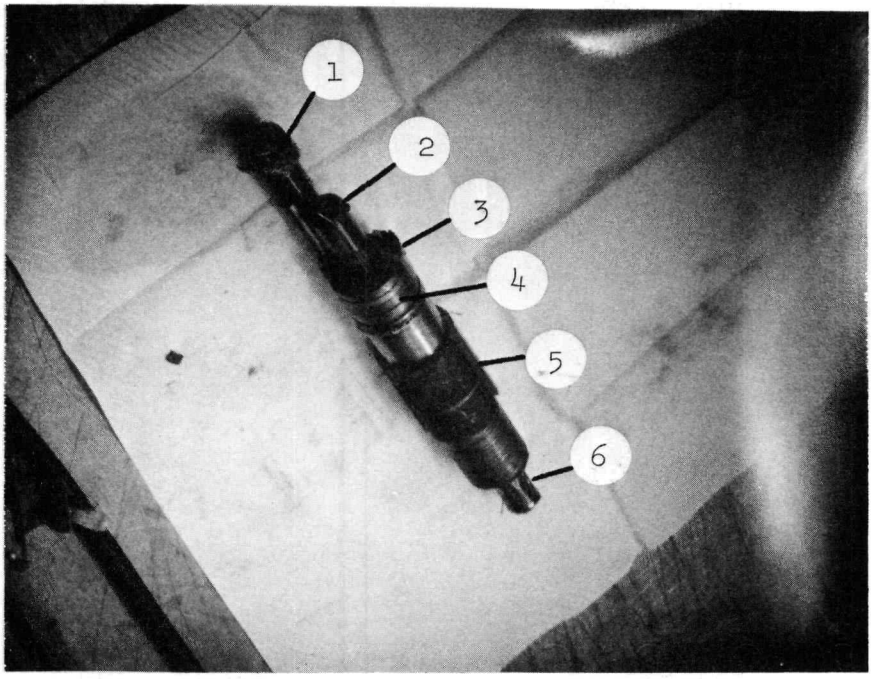

1. Emitter bus
2. Puncturing device
3. Collector bus
4. High temperature insulator seal
5. Collector and unbonded Al_2O_3 sheath insulator
6. Graphite sorption reservoir

Fig. 22. Converter IC-C3 after its removal from the primary containment

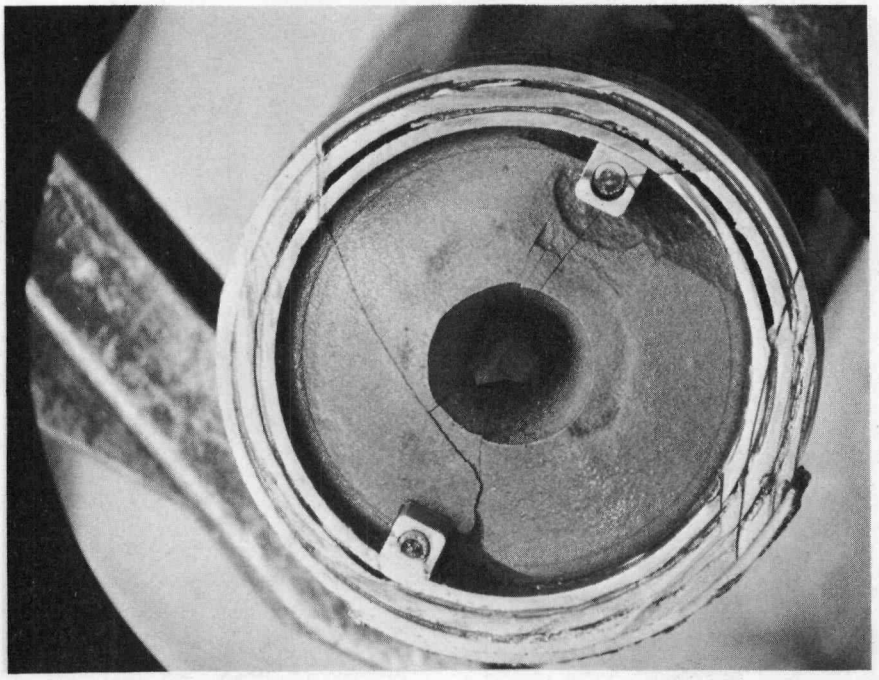

2.5X

Fig. 23. Appearance of the top of the fuel body of Converter IC-C3

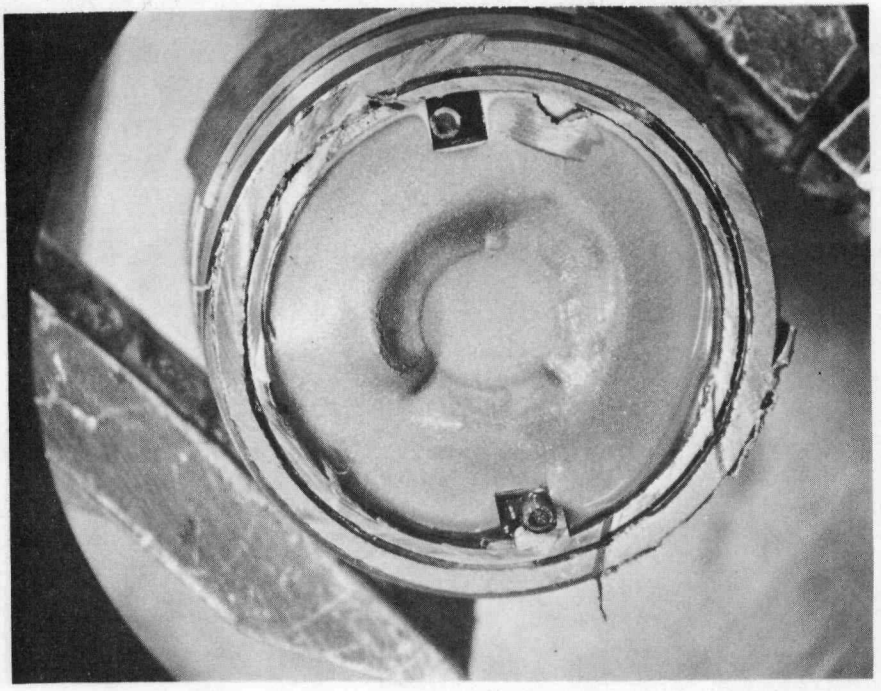

2.5X

Fig. 24. Appearance of the surface of the tungsten radiation shield in contact with the top of the fuel body of Converter IC-C3

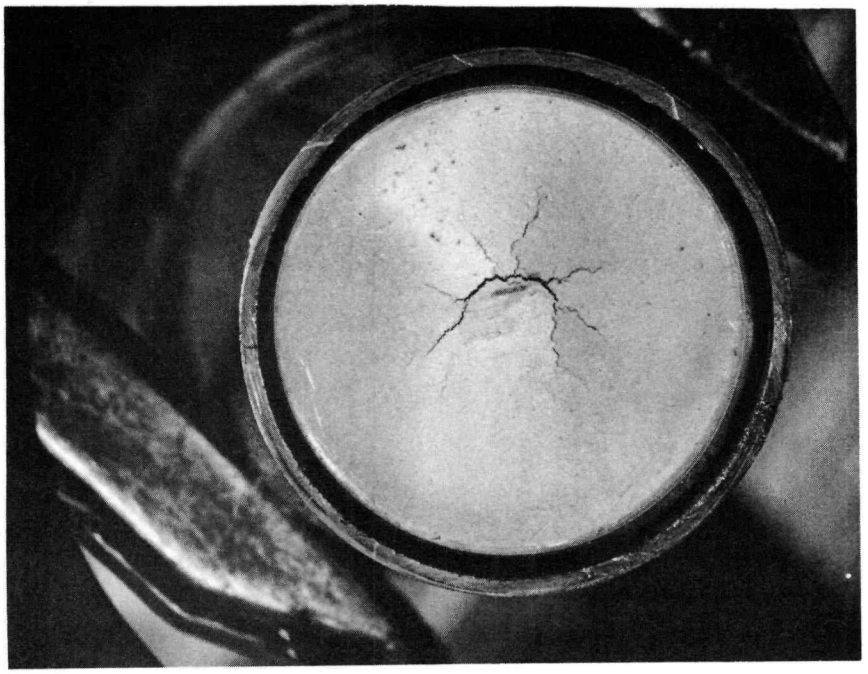

2.5X

Fig. 25. Appearance of the emitter bottom of Converter IC-C3

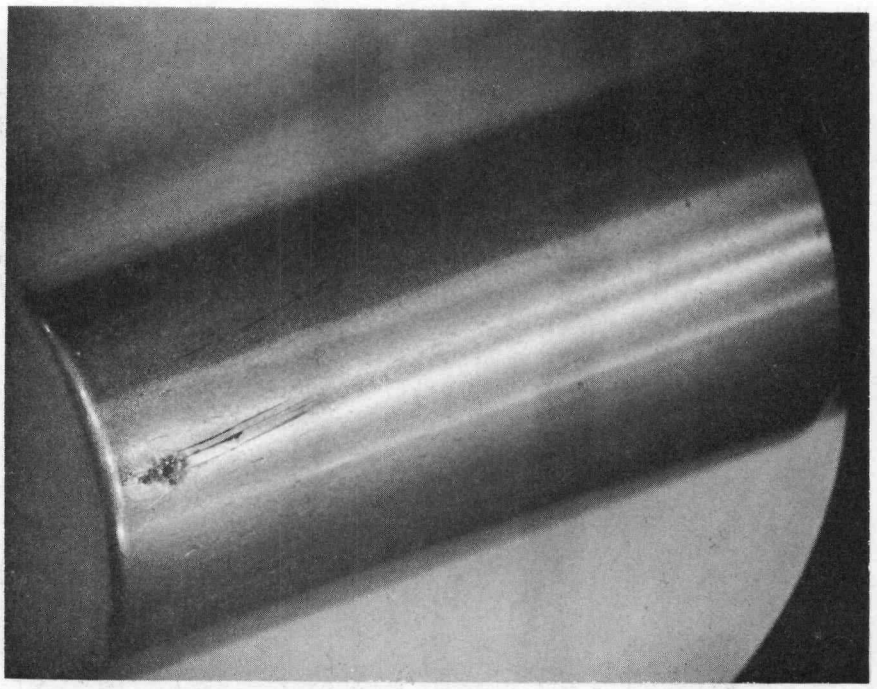

2.5X

Fig. 26. Appearance of emitter of Converter IC-C3. Note the point where the emitter was shorted to the collector. The marks were formed when the emitter was removed from the collector

short was partly caused by emitter expansion because of insufficient cold gap size between the fuel and the cladding, and partly due to a slight misalignment of the emitter with respect to the collector. To accommodate the differential expansion between the carbide fuel and the cladding at the outgassing temperature of 1720°C, a diametric cold gap of about 10 mil is needed between the fuel and the cladding, as estimated from the differential thermal expansion data reported recently.(1) The as-fabricated diametric cold gap size, however, was about 5.5 mils, resulting in a deficiency of 4.5 mils. Since then, the differential thermal expansion between the carbide fuel and tungsten has been determined and a more accurate estimate of the cold gap size required is now possible.

Table 5 lists the diameters of the emitter at a number of azimuthal and axial positions. It can be seen that the emitter expanded between 6 to 12 mils diametrically, with the maximum deformation located about 1/2 inch from the emitter bottom. Since the contribution of emitter diametrical expansion due to insufficient cold gap between the fuel and the emitter was 4.5 mils, the diametrical expansion due to fuel swelling is therefore between 1.5 to 7.5 mils, as compared to about a maximum of 4 mils for the Mark VI emitter of Converter IC-I3. The maximum deformation of the emitter bottom was found to be about 30 mils.

The emitter cavity was vacuum impregnated with an epoxy resin to protect the fuel body and then cut into two halves. The piece shown in Fig. 27 represents very closely one half of the emitter. The contour of the central venting channel (now filled with epoxy) reflects the amount of fuel swelling at different axial positions. This piece was mounted and polished to provide a longitudinal cross section view of the fueled emitter. Figure 28 shows such a view at a magnification of about 4X. Since the polishing removed about 80 mils of material from the surface, the view represents that of the cross section slightly below the bisecting plane of the emitter. A number of interesting features can be seen from Fig. 28.

TABLE 5

DIAMETERS OF TUNGSTEN EMITTER OF CONVERTER IC-C3
AFTER IN-PILE OPERATION (INCH)

(As-fabricated emitter diameter = 1.1009 inch)

Axial Position (inch from closed end emitter bottom)	Azimuthal Positions (see attached figure)		
	1-1	2-2	3-3
1/8	1.1069	1.1063	1.1080
1/4	1.1108	1.1113	1.1121
1/2	1.1122	1.1128	1.1113
3/4	1.1103	1.1116	1.1100
1	1.1095	1.1112	1.1102
1-1/4	1.1088	1.1102	1.1100
1-1/2	1.1110	1.1097	1.1099
1-3/4	1.1091	1.1095	1.1113
2	1.1092	1.1092	1.1095

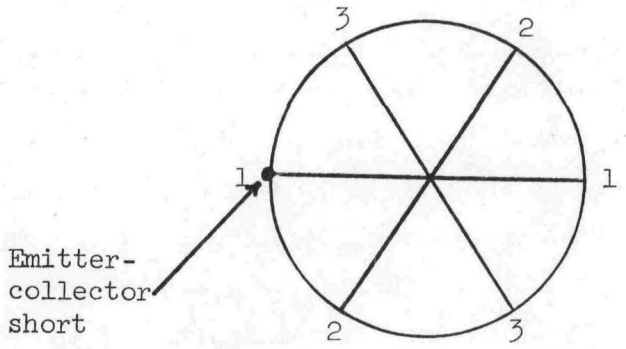

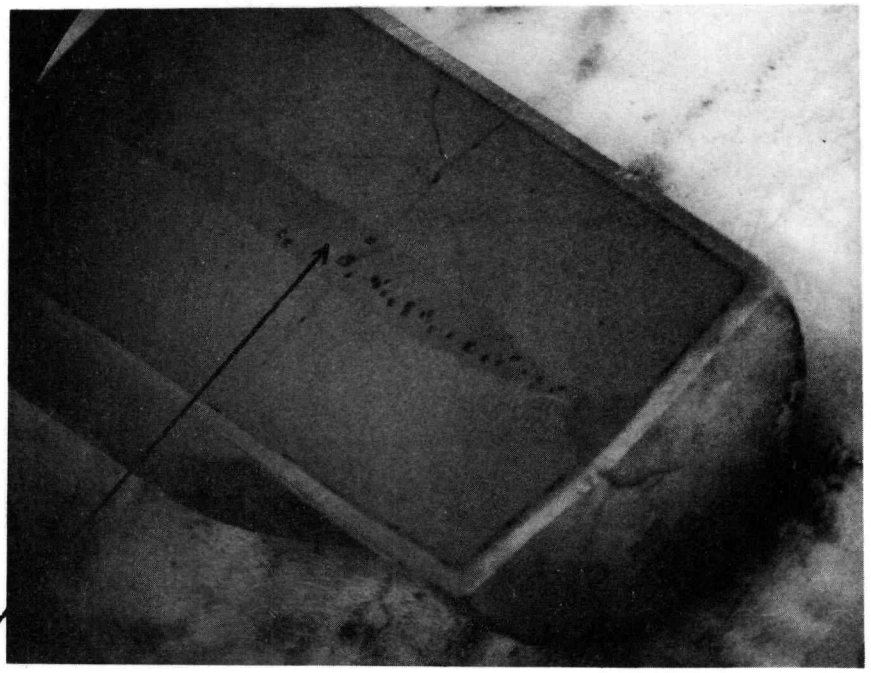

Central venting channel
filled with epoxy

2X

Fig. 27. One half of emitter of Converter IC-C3

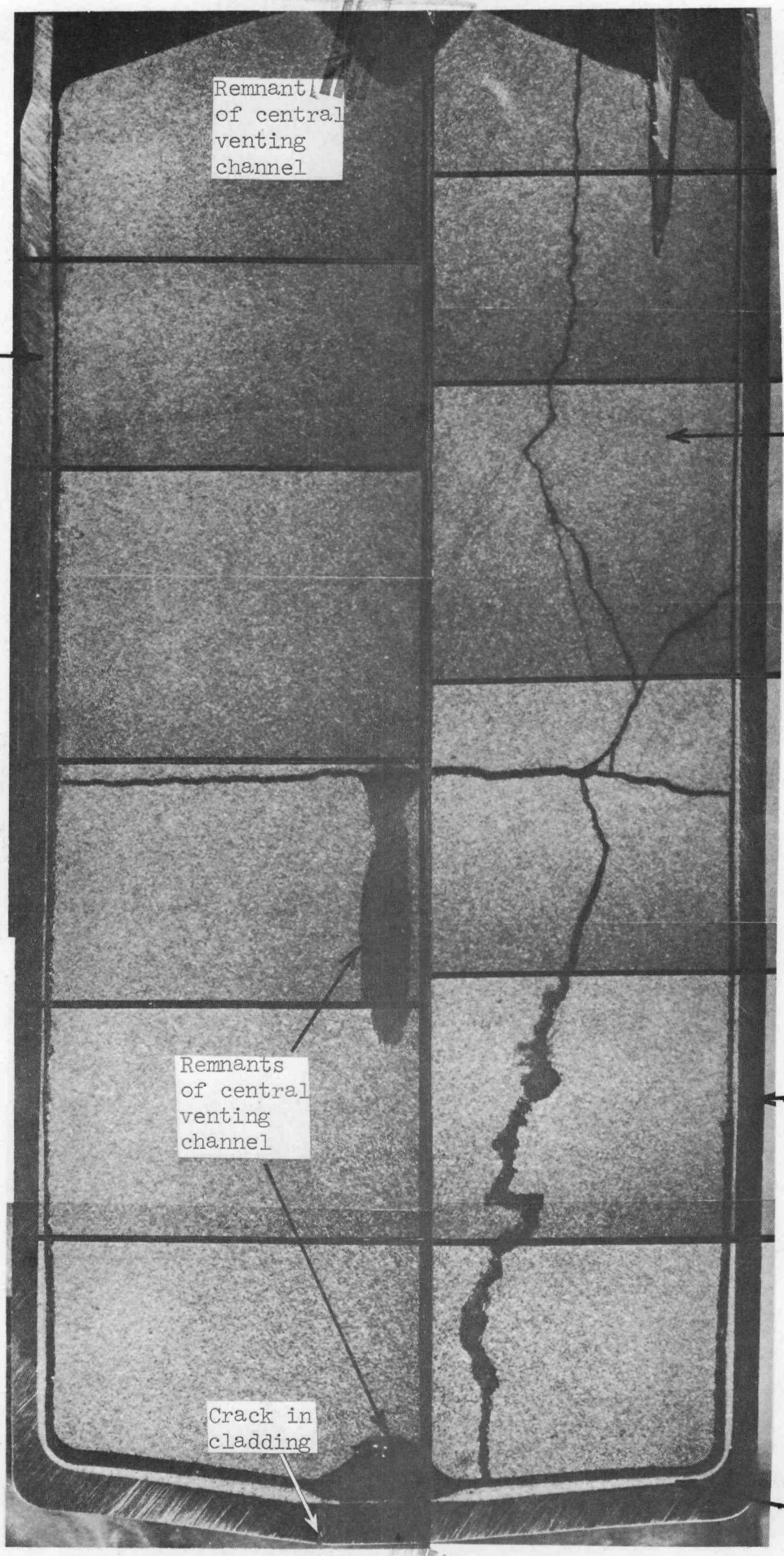

Fig. 28. Longitudinal cross section view of the fuel emitter of Converter IC-C3

(1) A reaction layer is present over all the fuel-cladding interface. The thickness varies from a few mils near the top of the emitter to about 20 mils near the center of the emitter bottom where the temperature is expected to be higher than that at the top of the emitter. This converter has no fuel pedestal. A pedestal is used now to keep the fuel from touching the emitter bottom.

(2) Fuel swelling has caused the expansion of the central portions of both the top and the bottom of the fuel body. The fuel cavity had a helium gas pressure of about 20 psi during operation. Both fuel swelling and gas pressure may have contributed to the deformation of the emitter bottom.

(3) A gross internal fabrication defect of about 3/4 inch length running in the longitudinal direction is present in the cladding.

(4) A crack is present in the cladding near the center of the emitter bottom. It was probably through this crack that the helium gas in the primary containment and the fuel cavity leaked into the interelectrode space to cause the termination of the test.

(5) The shape and the thickness of the reaction layer in Fig. 28 are similar to that of the black line observed at the fuel-cladding interface in the post-test neutron radiograph of this converter, (see Fig. 29). The interaction layer observed for Converter IC-I3 has been shown by electron microprobe analysis to be primarily the UWC_2 phase. This is most likely to be also true for the interaction layer of Converter IC-C3. The uranium-containing interaction layer absorbs more neutrons and leads to the formation of the black line in the neutron radiograph. Such a black line has also been observed in the neutron radiograph of Converter IC-C11 which also contains a carbide fueled tungsten emitter, and in the neutron radiograph of the Plum Brook Capsule V2-C which

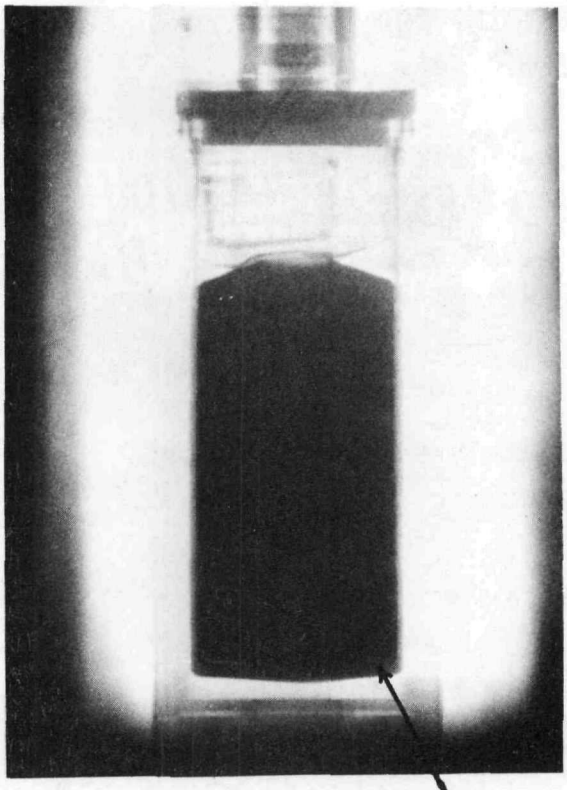

Black line due to the formation of uranium-containing fuel-cladding interaction layer (probably UWC_2 phase)

Fig. 29. Post-test neutron radiograph of Converter IC-C3. Note the black line at the fuel-cladding interface. (Natural size)

contains tungsten clad carbide fuel samples. All these observations indicate that the interaction between carbide fuel and tungsten cladding can be studied nondestructively and continuously in in-pile converters by following the distribution and the width of the black line at the fuel-cladding interface in the neutron radiographs taken of such converters. It is also interesting to note that although a black line was observed at the fuel-cladding interface in the neutron radiograph taken of Converter IC-C11, the performance of that converter did not change significantly during its 7500 hour operation. Perhaps the interaction layer formed does not have a strong influence on converter output. However, more tests should be made before a definite conclusion can be drawn.

Samples were taken from the counterpart of the piece shown in Fig. 28 for the study of the microstructures of the fuel and the cladding. Figure 30(a) is the macrophotograph of a sample taken near the bottom part of the emitter. The point where the emitter was shorted to the collector is about 1/16 inch underneath the location indicated in the figure. Examination at 50X magnification indicated the presence of a number of cracks in the cladding along the bottom and the corner of the emitter. The two largest ones which are also visible in Fig. 28, are shown in Figs. 30(b) and 30(c). It seems that the cracks were generated by the tensile stress induced in the cladding when the bottom of the emitter was pushed downward by fuel swelling and gas pressure in the emitter cavity. The reaction layer has the same columnar grain structures as that observed at the fuel-cladding interface of Converter IC-I3. Figure 31 shows the microstructures of the reaction layer at 150X magnification. Although no electron microprobe analysis was carried out, it is believed that the composition of the layer should be the same as that of the reaction layer of Converter IC-I3, since the reactants and the operation temperatures of these two converters are similar. Figures 32(a) and (b) are photomicrographs of the fuel-cladding interface of the bottom of the emitter, with the tungsten cladding etched to show the grain structures. Numerous precipitates (probably tungsten carbides) are seen at the grain boundaries of the cladding. The presence of such precipitates embrittled the grain

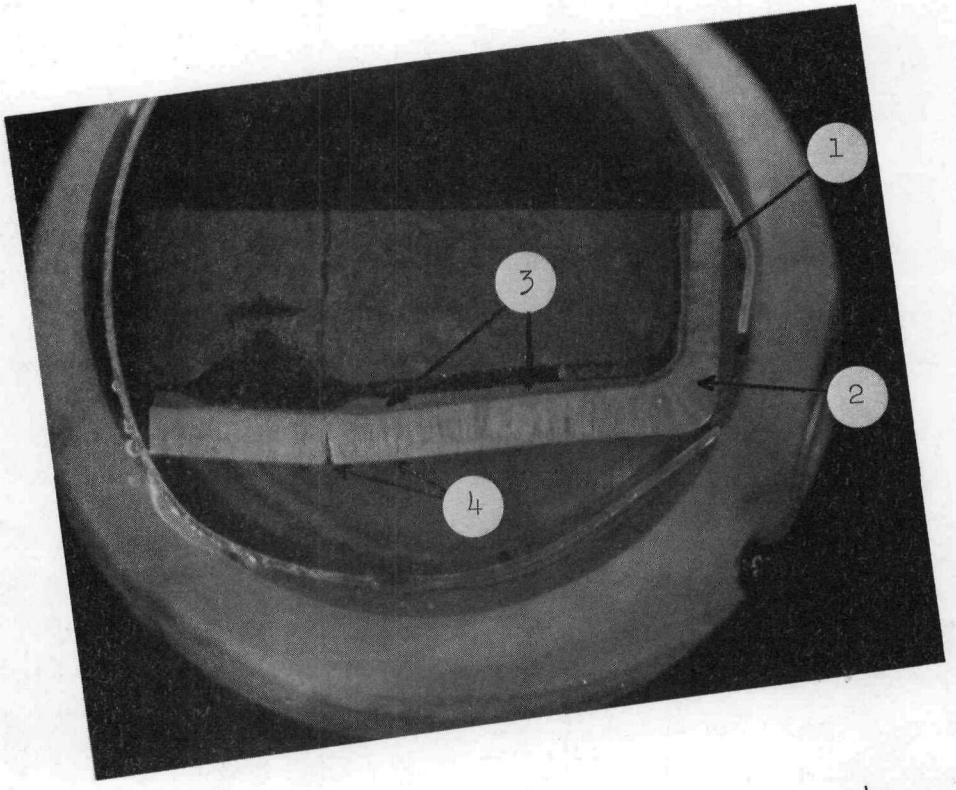

4X

1. Emitter-collector short occurred about 1/16 inch underneath this location
2. Tungsten cladding
3. Fuel-cladding interaction layer
4. Two large cracks

Fig. 30(a). Macrophotograph of the sample taken from the emitter bottom of Converter IC-C3 for microstructure examination

(b)

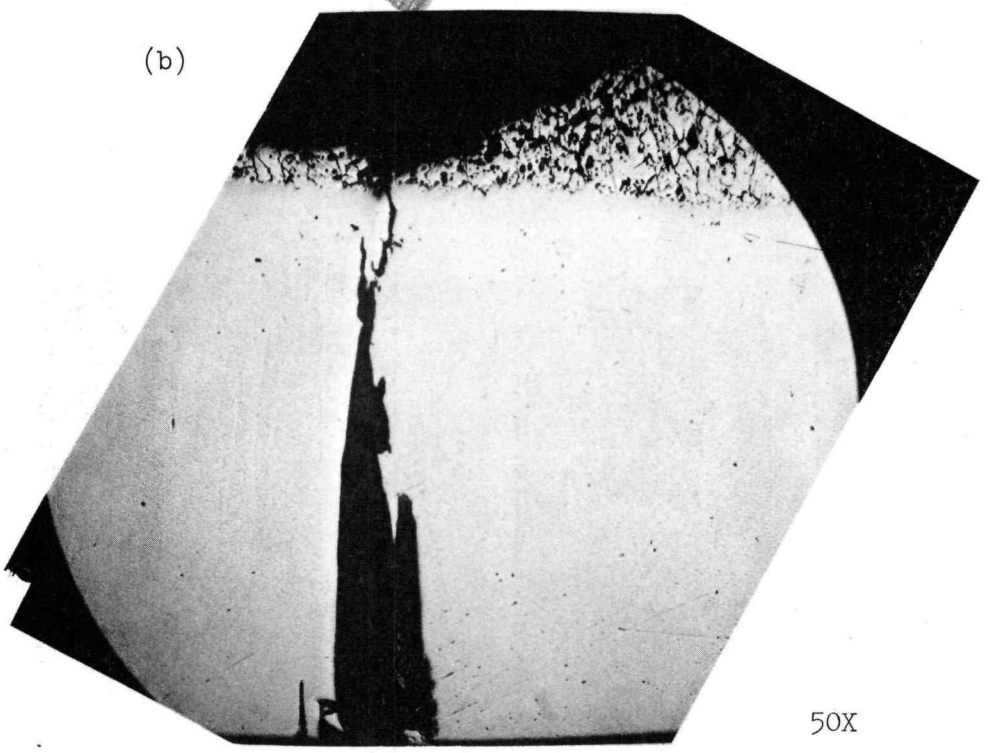

50X

(c)

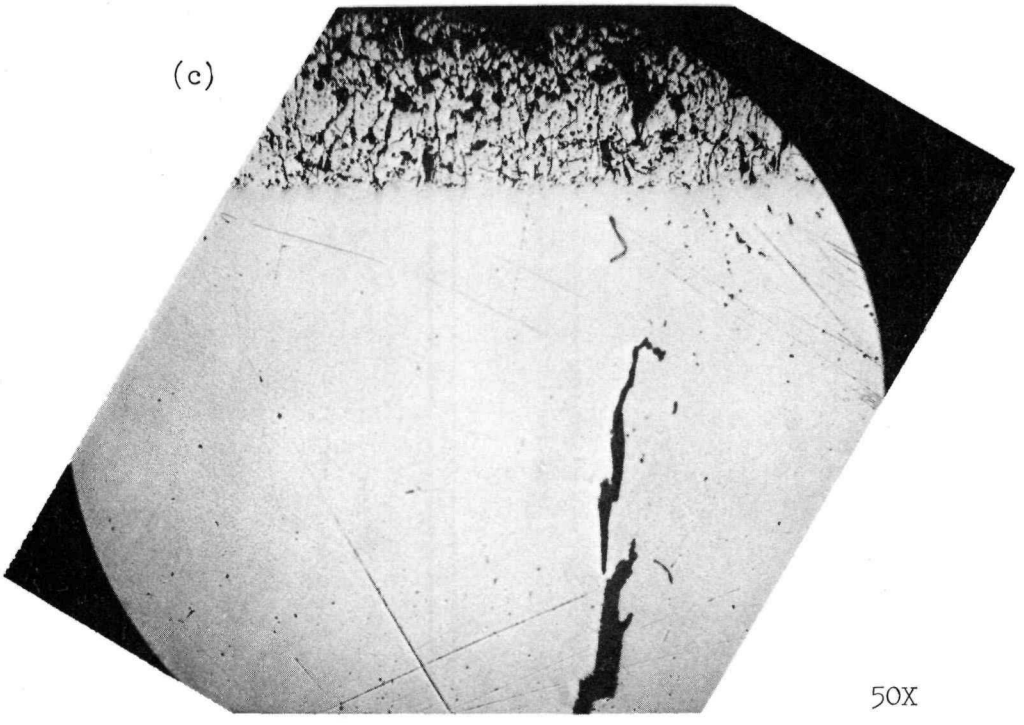

50X

Fig. 30(b) and (c). Two large cracks at the bottom of the emitter of Converter IC-C3

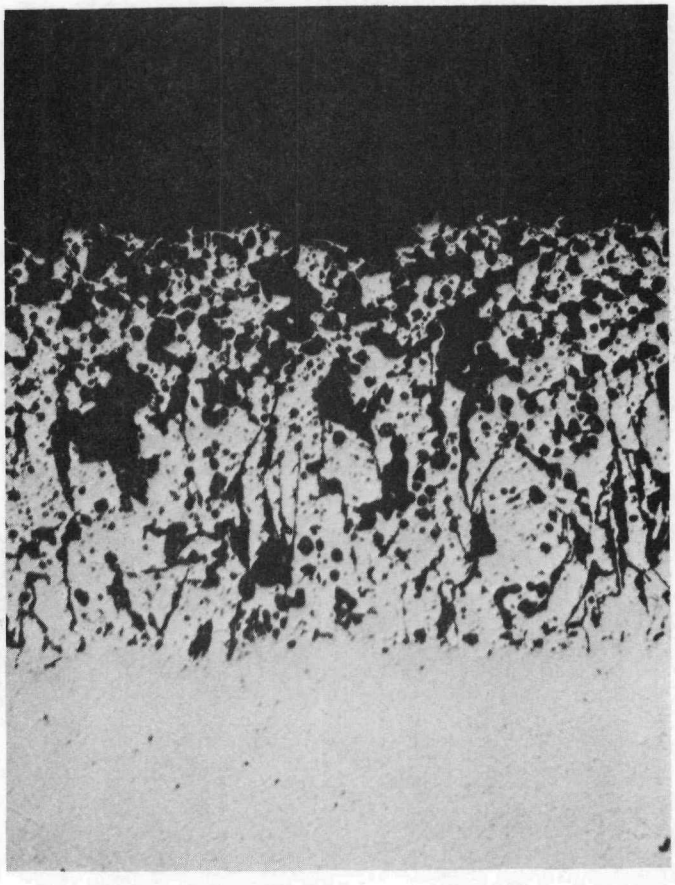

150X

Fig. 31. Microstructures of fuel-cladding interaction layer along emitter bottom of Converter IC-C3

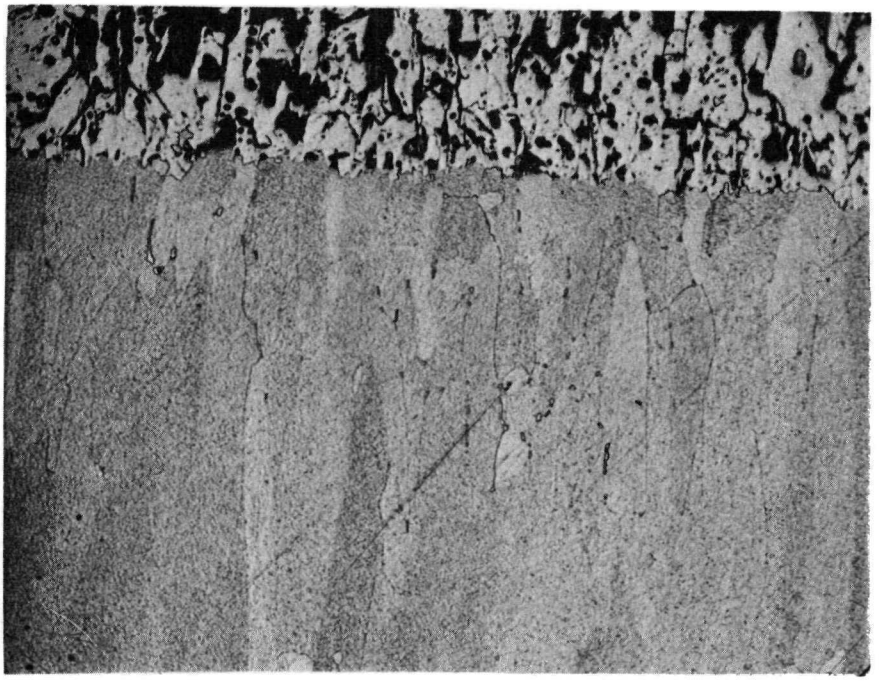

(a) Near the crack in Fig. 30(c) 150X

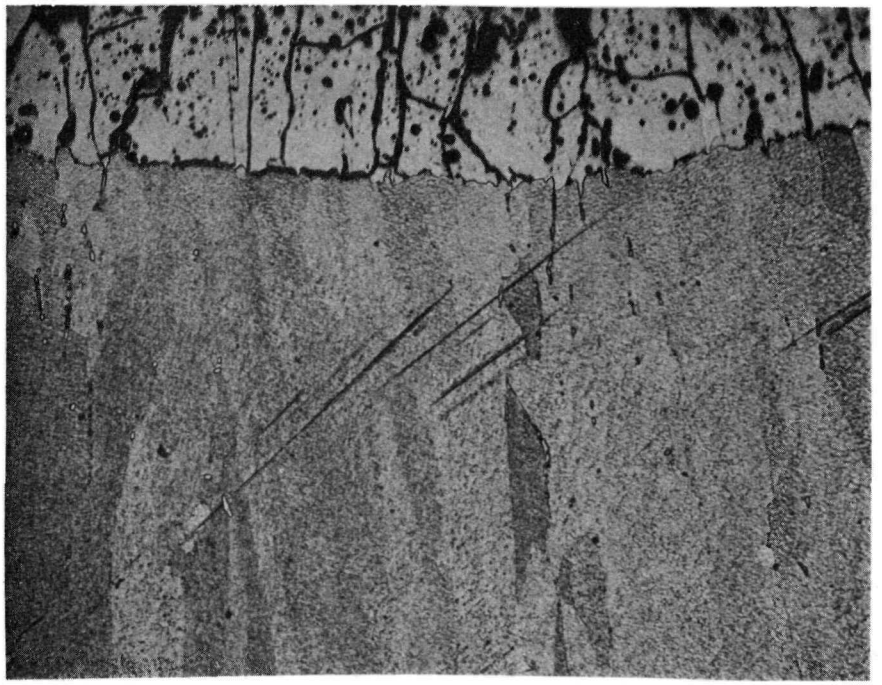

(b) To the right of the crack in Fig. 30(b) 150X

Fig. 32. Microstructures of fuel-cladding interface of emitter bottom of Converter IC-C3 (etched). Note precipitates in grain boundaries of tungsten cladding

boundaries and caused the cracking of the emitter bottom when the latter was stressed by fuel swelling and gas pressure in the fuel chamber. In contrast to the above observation, no grain boundary precipitates were found in the tungsten cladding of a sample taken from the cylindrical part of the emitter, which was about one inch up from the emitter bottom (Fig. 33). The more severe fuel-cladding interaction at the emitter bottom is probably caused by the higher temperature there. The lack of electron cooling at the emitter bottom and the absence of a fuel pedestal all contributed to the higher temperature and the presence of a high stress at the emitter bottom aggravated the situation. The failure of the cladding is thus a type of high temperature stress corrosion cracking or stress corrosion fatigue cracking when the emitter bottom is thermally cycled. Efforts were made to examine the damage in cladding structures in the vicinity of the short to the collector but none was found. The stain observed on the emitter at the point where the short occurred, as shown in Fig. 26, is only surface in nature. Figure 34 shows the typical microstructures of the carbide fuel material facing the interaction layer at the bottom of the emitter. The fuel seems to be highly porous and contains fission gas bubbles and a dispersion of a light-colored second phase (probably UWC_2).

The niobium collector was sectioned into two halves (Fig. 35), with the location where the collector was shorted to the emitter indicated. Most of the collector surface was covered with a dark film. At the point where the short occurred, a reaction layer containing cracks was observed (Fig. 36(a)). The layer became thinner and more uniform as the distance from the point of collector-emitter shortage increased (Fig. 36(b)). Figure 36(c) shows the etched appearance of the reaction zone. It can be seen that there are two layers in the reaction zone. From the appearance of the etched reaction layers and their polishing characteristics, it is concluded that the two reaction layers are most-likely the niobium carbides Nb_2C and NbC. Although no other collector samples were examined, it is believed that the carbide layer is present over most of the collector surface. In fact, a carbide layer was found on the inside surface of the lower niobium skirt brazed to the top of the collector. The source of the carbon could be the carbide fuel material or the carbon in the graphite sorption reservoir. The carbon

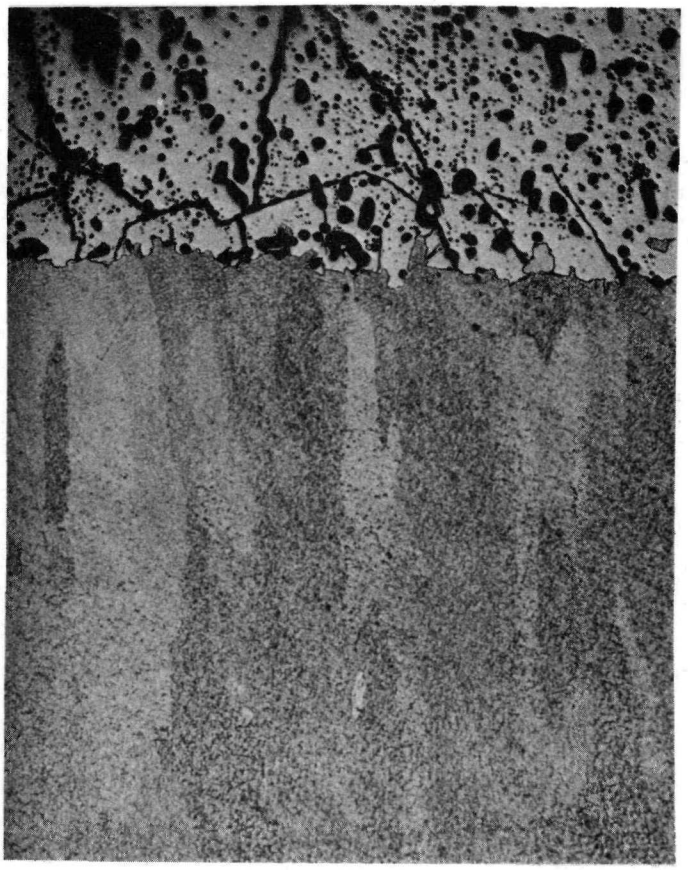

150X

Fig. 33. Microstructures of fuel-cladding interface at location about one inch up from the emitter bottom of Converter IC-C3. Note no grain boundary precipitates

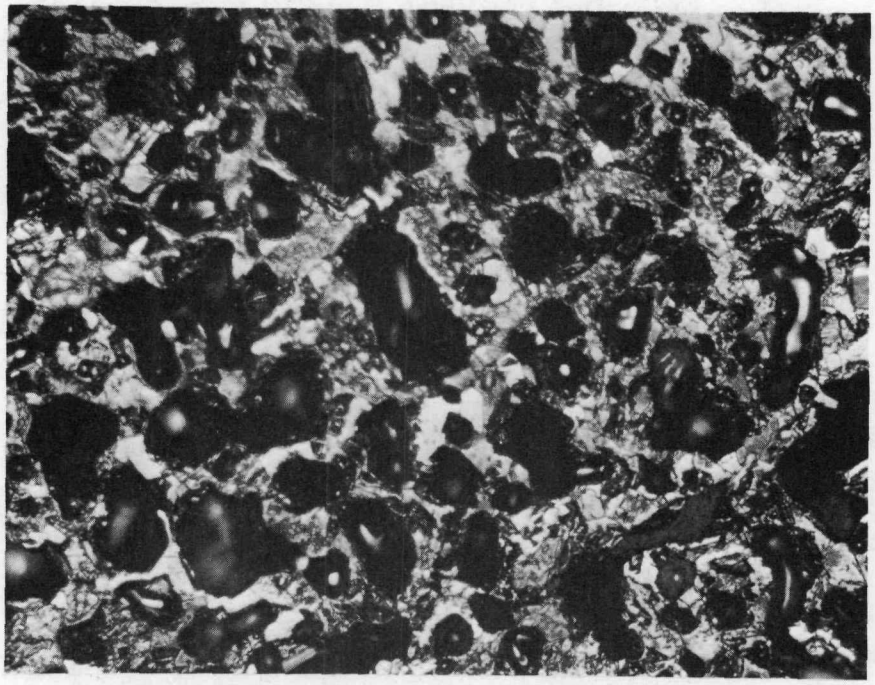

350X

Fig. 34. Typical microstructures of irradiated carbide fuel material in Converter IC-C3

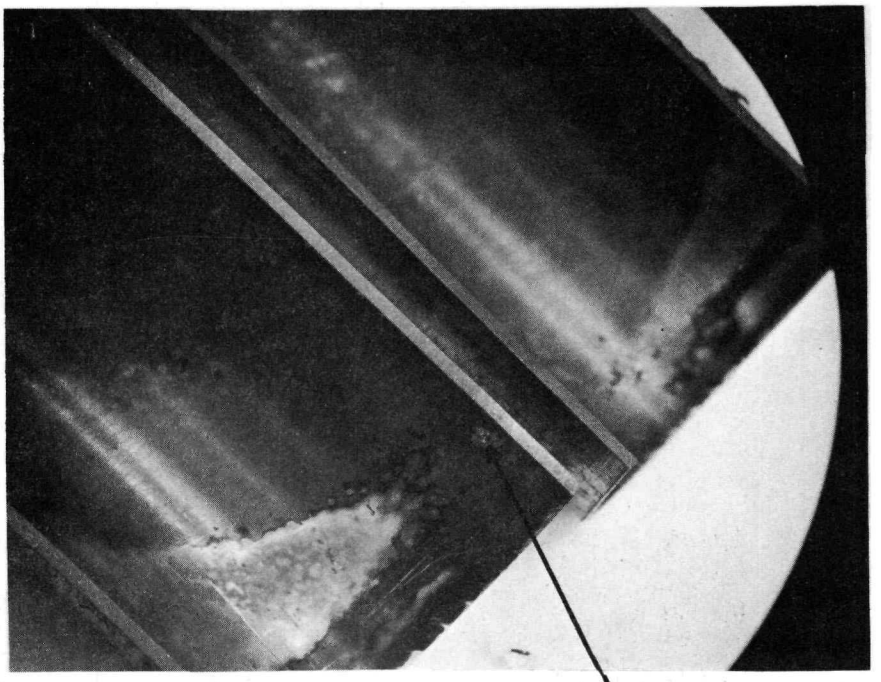

Fig. 35. Two halves of the niobium collector of Converter IC-C3 after sectioning

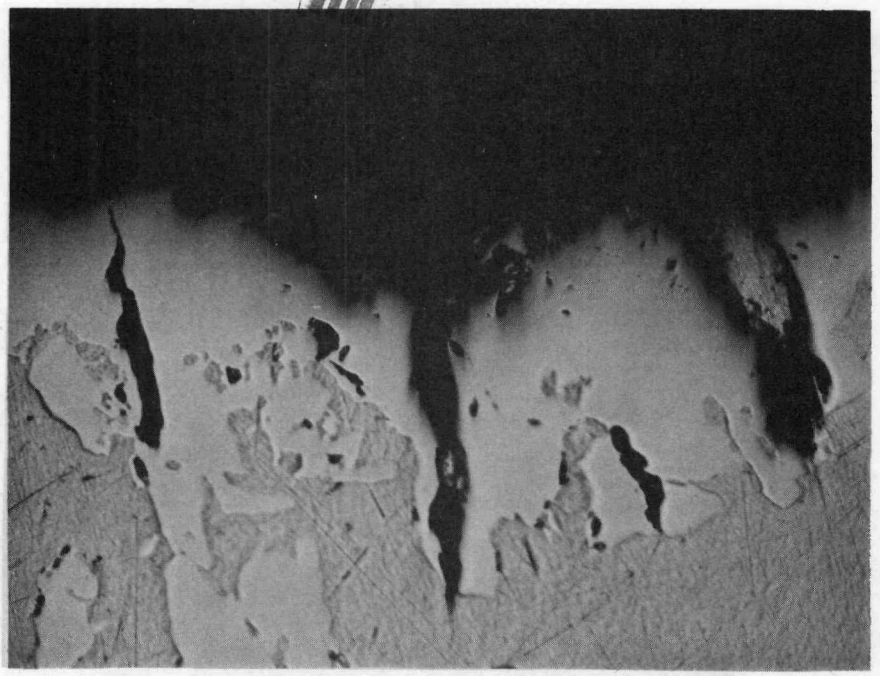

300X

(a) At the point where the collector was shorted to the emitter

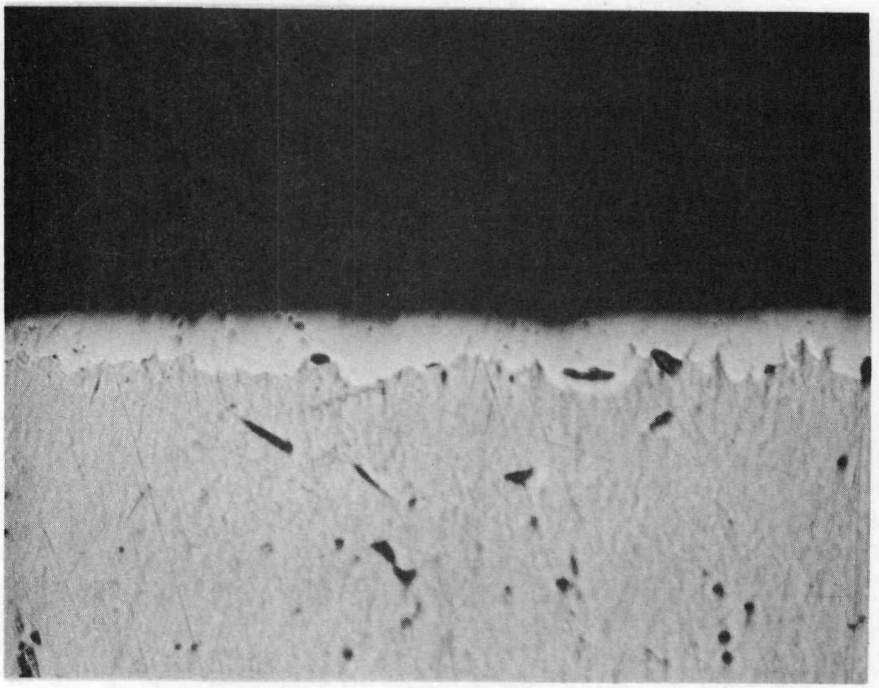

300X

(b) At a distance of about 1/4 inch away from that for (a). The layer is compact and fairly uniform and from 0.5 to 1 mil in thickness

Fig. 36. Appearance of the reaction layer on the niobium collector surface of Converter IC-C3. (Sheet 1 of 2)

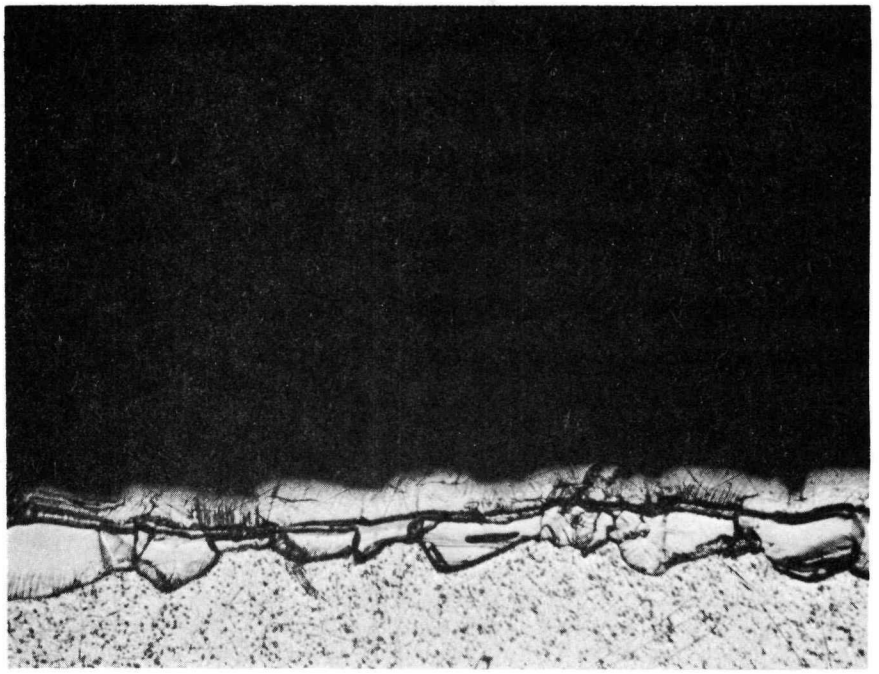

300X

(c) Etched appearance of the reaction zone. Note the presence of two layers in the reaction zone

Fig. 36. Appearance of the reaction layer on the niobium collector surface of Converter IC-C3. (Sheet 2 of 2)

in the carbide fuel could arrive at the collector surface by diffusion through the tungsten cladding and the carbon from the graphite reservoir could arrive at the collector surface by vaporization or transport through the vapor phase by an impurity carrier (such as the formation of CO with oxygen impurity). However, since an out-of-pile unfueled converter (A-4) containing a graphite sorption reservoir has demonstrated stable performance for over 10,000 hours under similar operation conditions, it seems that the major portion of the carbon arriving at the collector surface was derived from the carbide fuel material. This conclusion is also substantiated by the observation that no carbide layer was detected on the inside surface of the upper niobium skirt of the insulator seal. If carbon can be transported from the graphite sorption reservoir as CO, then it should also be able to reach the inner surface of the upper niobium skirt and carburize it. A conclusive answer to the carbon transport from the graphite sorption reservoir to all converter component has to wait for the post-operational examinations of the A-4 converter.

Figures 37(a) and (b) shows the appearance of a cross section of the high temperature insulator seal. It can be seen that the metallizing layer is intact and the bond between the niobium skirt, braze and Lucalox is good.

Figure 38 contains the graphite pieces recovered from the graphite sorption reservoir. The original loading consisted of four cylinders of 1/4 inch diameter and 3/8 inch length. It can be seen the most of the graphite cylinders have delaminated into thin wafers. This has also been observed out-of-pile when such graphite cylinders were loaded with cesium. These cylinders are formed by pressing crossly laid layers of graphite fibers. The traces of the edges of these layers appear as wavy lines on the cylindrical surface of the cylinder and the fibers oriented at different directions appear as "domains" on the horizontal cross section of the cylinder, (see Fig. 38). Figure 39(a) shows the view of a horizontal cross section of a graphite cylinder. It can be seen that no separation has occurred among the fibers or between the domains of differently oriented fibers. The light-colored materials are the binders used during the fabrication of the graphite cylinder. Figure 39(b) shows a view of a longitudinal

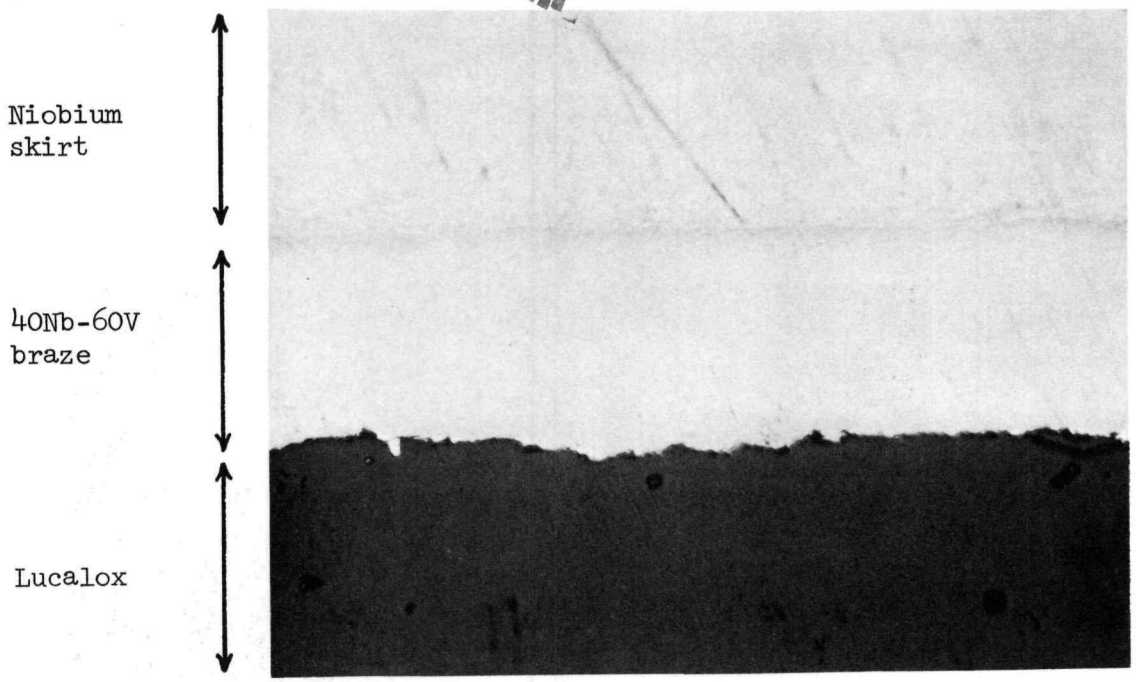

350X

(a) Unetched. Good bond between niobium, braze and Lucalox

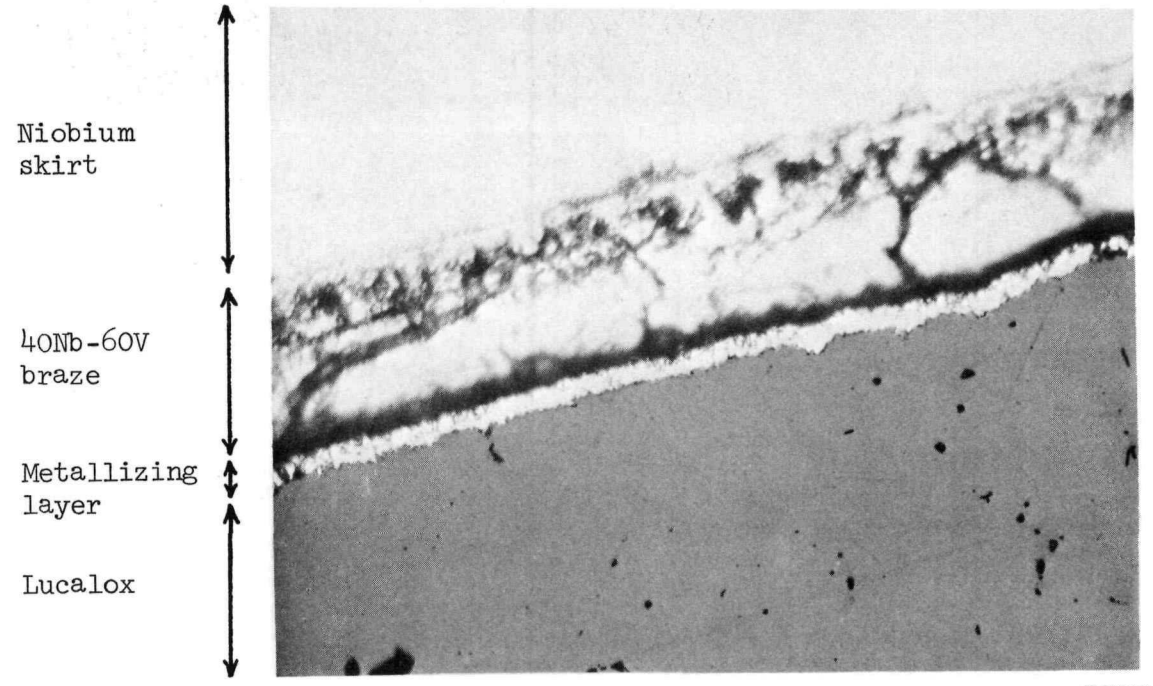

350X

(b) Etched. The metallizing layer is intact and the bond between the metallizing layer and Lucalox is good

Fig. 37. Appearance of a cross section of the high temperature insulator seal in Converter IC-C3

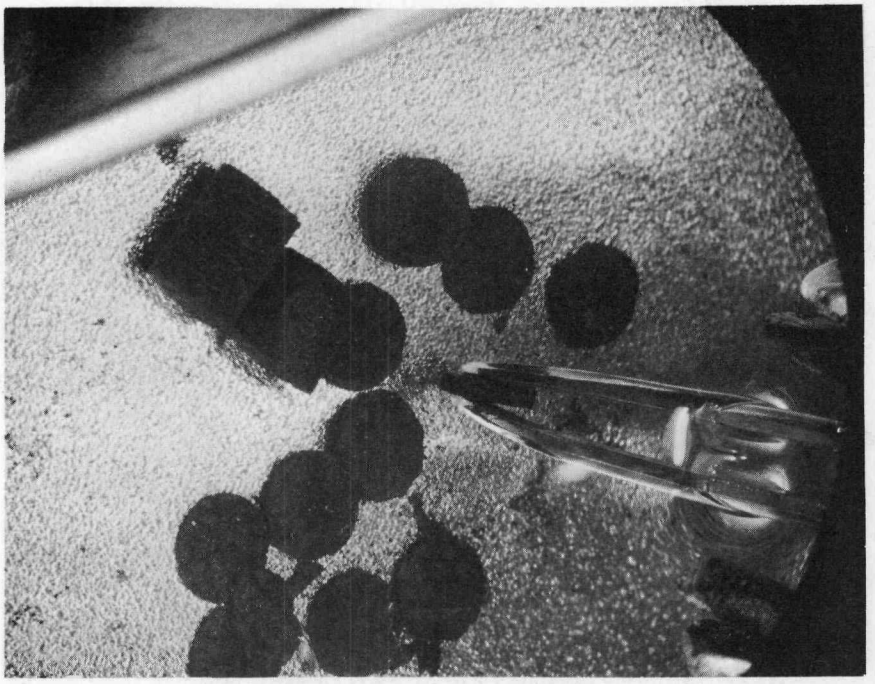

2X

Fig. 38. Graphite pieces recovered from the graphite sorption cesium reservoir in Converter IC-C3

400X

(a) Horizontal cross section view. No separation between graphite fibers or groups of differently oriented graphite fibers

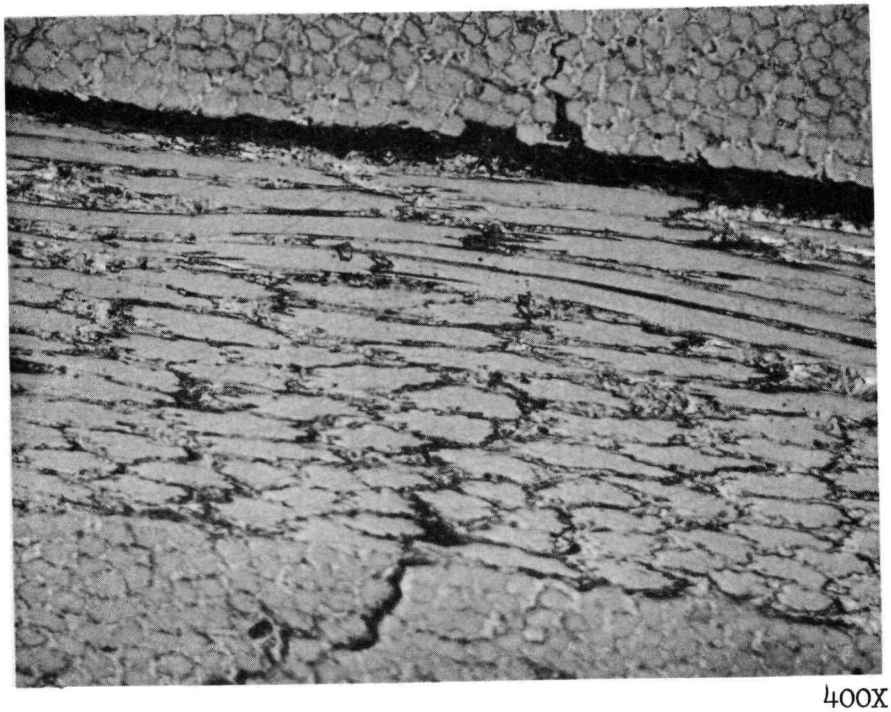

400X

(b) Longitudinal cross section view. Separations along planes containing the long graphite fibers

Fig. 39. Cross section views of a graphite cylinder used in sorption cesium reservoir in Converter IC-C3

cross section of a graphite cylinder. It can be seen that separation has occurred along planes containing the long graphite fibers. Examination of the inner surface of the niobium container of the graphite cylinders indicated the presence of a thin (~ a few tenths of a mil) carbide layer. It seems that niobium is a satisfactory material for containing the graphite pieces for sorption reservoir application.

Figure 40 is a photomicrograph of the interface between the tantalum transition piece and the tungsten emitter stem. The bond (which is estimated to operate at about 1200°C) appears to be in excellent shape and no Kirkendall void can be seen at the interface. The result adds further confidence to the use of such a joint in thermionic fuel element design.

CONCLUSIONS

On the basis of the hot cell examination results for Converters IC-I3 and IC-C3, the following conclusions can be drawn.

(1) The presence of tungsten thermocouple wells in the emitter cavity is undesirable, since it imposes stress concentrations on the emitter cladding when fuel swelling occurs. Tungsten thermocouple wells have been eliminated from all the converters fabricated since IC-C14.

(2) The use of a fuel pedestal helps to reduce the temperature of the emitter bottom and to alleviate the interaction between the fuel and emitter bottom where the stress due to fuel swelling is expected to be higher than that elsewhere in the cladding. Fuel pedestals have been used in all the converters fabricated since IC-C3.

(3) The carbide fuel of C/U atom ratio = 1.05 tends to react with the tungsten cladding and to embrittle the cladding, especially in the presence of stress. The C/U atom ratio of the carbide fuel has been lowered to 1.03 for the last five fuel loadings used in the 6F thermionic fuel element.

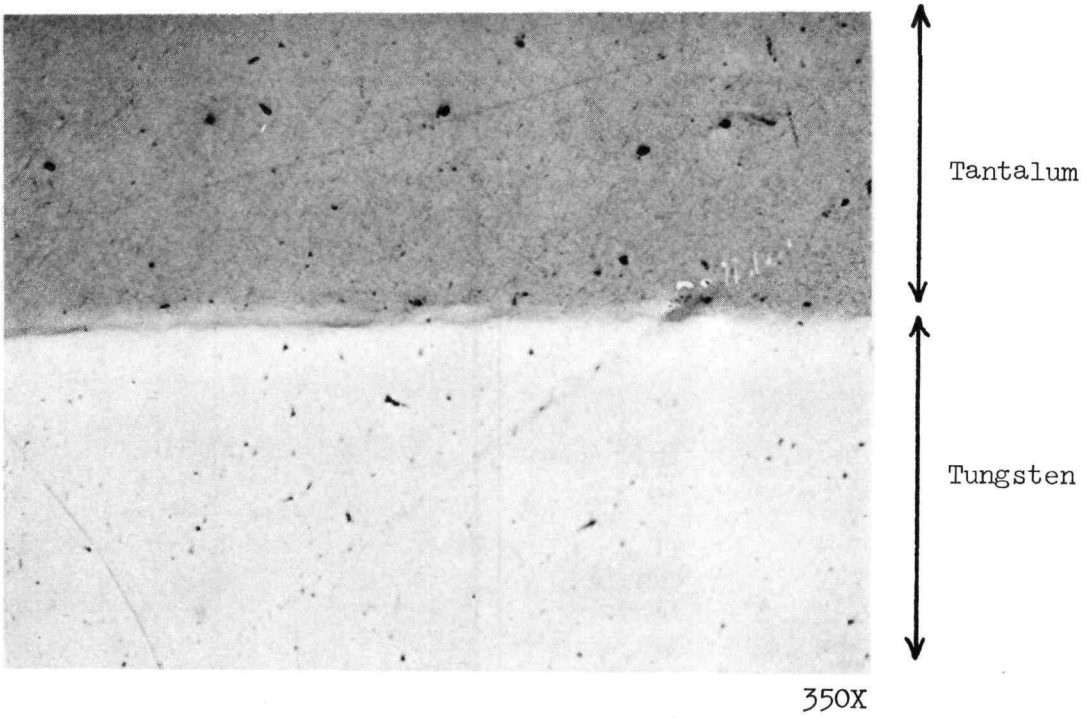

Fig. 40. Appearance of the interface between the tantalum transition piece and the tungsten emitter stem in Converter IC-C3

(4) The tantalum to tungsten diffusion bond has remained intact during in-pile tests of these two converters. No serious problem is expected in using such a joint in thermionic fuel element design.

(5) The high temperature insulator seal has performed satisfactorily. The appearances of the braze and the metallizing layer lend confidence to the use of such an insulator seal in thermionic fuel element design.

(6) Niobium is a satisfactory container material for the graphite pieces used in sorption cesium reservoirs.